Journal of Materials Chemistry A

REVIEW

View Article Online
View Journal | View Issue

Cite this: J. Mater. Chem. A, 2021, 9, 19346

Hybrid artificial photosynthetic systems constructed using quantum dots and molecular catalysts for solar fuel production: development and advances

Jing Liu,† Ying-Yi Ren,† Jin Wu, Wu Xia, Bo-Yi Deng and Feng Wang *

The construction of artificial photosynthetic (AP) systems for the hydrogen evolution reaction (HER) and carbon dioxide reduction reaction (CRR) is one of the hottest topics in the field of energy and sustainability. A typical AP system is composed of three key components, a photosensitizer (PS) for visible light harvesting, a catalyst for redox reactions, and a sacrificial electron donor (SED) for consuming holes generated in the PS. Among these three components, the PS and catalyst affect the photocatalytic performance much. There are two main types of AP systems, heterogeneous systems using inorganic materials and homogeneous systems using molecules. In addition to these, a compromise strategy of using inorganic luminescent nanoparticles as photosensitizers and molecular metal complexes as catalysts to construct hybrid AP systems has been developed. Inorganic luminescent nanoparticles, such as colloidal quantum dots (QDs) and carbon quantum dots (CQDs), have advantages of robust photostability, multiple excitation, and easy preparation. Molecular catalysts feature high activity, modifiable structures, and atom economy. Research on the combination of these two different types of materials to construct hybrid systems for solar fuel production is blooming. In the last decade, a large number of hybrid AP systems have been reported, and various strategies for system construction were developed. Obvious improvements in the photocatalytic efficiency of solar fuel production were witnessed. This review focuses on hybrid AP systems for the HER and CRR. The mechanism, composition, system design, and photocatalytic performances of the reported hybrid AP systems are reviewed. The advances and challenges in this field are discussed.

Received 31st March 2021
Accepted 27th June 2021

DOI: 10.1039/d1ta02673a

rsc.li/materials-a

Key Laboratory of Materials Chemistry for Energy Conversion and Storage (Huazhong University of Science and Technology) of Ministry of Education, Hubei Key Laboratory of Material Chemistry and Service Failure, Hubei Engineering Research Center for Biomaterials and Medical Protective Materials, School of Chemistry and Chemical Engineering, Huazhong University of Science and Technology, Wuhan, 430074, P. R. China. E-mail: wangfengchem@hust.edu.cn

† These two authors contributed equally to this review.

Jing Liu received his B.S. degree in Chemical Engineering and Technology from the Wuhan University of Science and Technology. He is currently in his second year as a graduate student in Materials Chemistry under the supervision of Associate Professor Feng Wang in the School of Chemistry and Chemical Engineering, Huazhong University of Science and Technology. He is currently working on artificial photosynthetic H_2 production and CO_2 reduction.

Ying-Yi Ren received her B.S. degree in Materials Chemistry from Shanxi University. She is currently in her second year as a graduate student in Materials Chemistry under the supervision of Associate Professor Feng Wang in the School of Chemistry and Chemical Engineering, Huazhong University of Science and Technology. Her current work focuses on artificial photosynthesis.

1. Introduction

Green plants and some bacteria and algae on Earth carry out photosynthetic reactions everyday, and these are the largest scale photochemical reactions occurring around us.[1–4] Photosynthesis not only provides energy for the growth of plants but also balances the concentration of carbon dioxide (CO_2) and oxygen (O_2) in the atmosphere. The essence of photosynthesis is that plants store solar energy in chemical bonds *via* solar-to-chemical energy conversion. In the view of human beings, this process is a green, sustainable, and ideal way of solar energy utilization (Scheme 1).[5–7] Inspired by photosynthesis in nature, scientists proposed, as early as in the 1910s,[8] to construct artificial photosynthetic systems to make fuels and chemicals in a green and clean way.[9–13] Giacomo Ciamician, a photochemist in Italy, wrote in an essay titled "The photochemistry of the future" published in 1912 that "On the arid lands there will spring up industrial colonies without smoke and without smokestacks; forests of glass tubes will extend over the plains and glass buildings will rise everywhere; inside of these will take place the photochemical processes that hitherto have been the guarded secret of the plants, but that will have been mastered by human industry which will know how to make them bear even more abundant fruit than nature, for nature is not in a hurry and mankind is. And if in a distant future the supply of coal becomes completely exhausted, civilization will not be checked by that, for life and civilization will continue as long as the sun shines!" The pioneering study on artificial photosynthesis emerged in the 1970s. Fujishima and

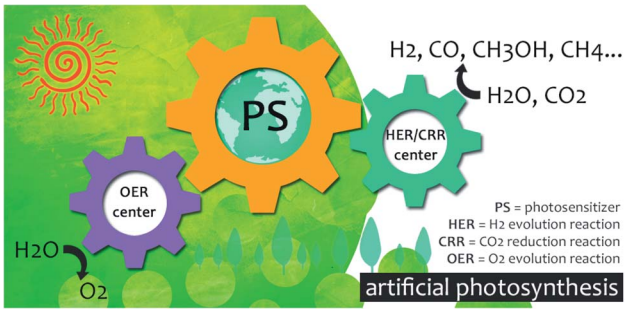

Scheme 1 Schematic diagram of artificial photosynthesis.

Jin Wu received his B.S. degree in Pharmaceutical Engineering from Hefei Normal University. He is currently in his third year as a graduate student in Materials Chemistry under the supervision of Associate Professor Feng Wang in the School of Chemistry and Chemical Engineering, Huazhong University of Science and Technology. He focuses on developing self-assembly systems for photocatalytic H_2 production and CO_2 reduction.

Bo-Yi Deng received his B.S. degree in Materials Chemistry from the Nanjing University of Science and Technology. He is currently in his first year as a graduate student in Materials Chemistry under the supervision of Associate Professor Feng Wang in the School of Chemistry and Chemical Engineering, Huazhong University of Science and Technology. He is working on supramolecular photoluminescence.

Wu Xia received his B.S. degree in Chemistry from Hubei Engineering University and M.S. degree in Organic Chemistry from Hubei University. He is currently a PhD candidate in Organic Chemistry under the supervision of Associate Professor Feng Wang in the School of Chemistry and Chemical Engineering, Huazhong University of Science and Technology. His current work focuses on photocatalytic CO_2 reduction.

Feng Wang received his B.S. degree in Applied Chemistry from the Huazhong University of Science and Technology in 2005 and his Ph.D. from the Technical Institute of Physics and Chemistry, the Chinese Academy of Sciences, under the supervision of Professor Li-Zhu Wu and Professor Chen-Ho Tung in 2013. After postdoctoral research (2013–2016) at the University of Hong Kong, working with Professor Chi-Ming Che, he joined the faculty of Huazhong University of Science and Technology as an Associate Professor. His research interests include artificial photosynthesis, self-assembly of optical-functional materials, and supramolecular photoluminescence.

Honda reported that water can be photo-electrochemically split into H_2 and O_2 by irradiation of an electrochemical cell using TiO_2 and platinum black as the anode and cathode, respectively.[14] In recent decade, a research blooming of artificial photosynthesis is witnessed because of the concern on fossil energy depletion and environmental pollution by human society.

The study of artificial photosynthesis focuses mainly on two half-reactions, the HER and CRR. The products of these two reactions, such as H_2, carbon monoxide (CO), methanol (CH_3OH), methane (CH_4), *etc.*, are energy-bearing molecules and referred to as solar fuels.[15,16] The HER is a two-electron-reduction reaction involving two protons and one H–H bond formation. In contrast, the CRR is complex. The CRR produces different products depending on the number of electrons participating in it (Scheme 2). In most of the cases, the HER is an inevitable competing reaction in the CRR system.

A typical AP system contains at least three key functional components, a photosensitizer, a catalyst, and a sacrificial electron donor. The PS harvests visible light and generates excited electrons of high potential. Semiconductors,[17–21] organic dyes,[22–24] and noble metal complexes[25–28] are usually used as PSs in AP systems. The catalyst is the active site for the HER or CRR. There are two categories, molecular catalysts (MC)[29–32] and non-molecular catalysts, such as inorganic nanomaterials.[33–35] The molecular catalysts are those molecules and macromolecules having a definite chemical structure, such as transition metal complexes or macromolecules/polymer containing metal complexes as catalytic centers. The SED provides electrons for photocatalysis. Water (H_2O) is an ideal SED for AP systems. However, in most of the cases, small organic molecules that are easily oxidized, such as ascorbic acid (AA), triethylamine (TEA), triethanolamine (TEOA), and isopropanol (IPA), are used as alternatives due to the high oxidation potential of water.

In the past few decades, various materials have been used to construct AP systems. According to the types of materials, the AP systems can be divided into three types. The first type is a heterogeneous AP system, which is composed of inorganic materials, such as semiconductors, metal oxides, MOFs, COFs and their composites. The second type is a homogeneous AP system. In this type, both the photosensitizer and catalyst are molecules, and two functional components are physically mixed to construct an intermolecular system or covalently linked/self-assembled together to form an intramolecular system. The third type of AP system is a hybrid system, which is commonly composed of colloidal quantum dots (QDs) as a PS and a transition metal complex as a catalyst. This type of system is developed as an alternative to the homogeneous system. The latter suffered from low turnovers and stability due to fast decomposition of the molecular PS, such as noble-metal complexes and organic dyes, under light irradiation and high efficiency of charge recombination between the molecular PS and MC.[36–38]

There are many excellent reviews on the first two types of AP systems.[39–43] Studies on hybrid AP systems developed rapidly after the first such system described by the Wu group in 2011.[44] In the last decade, a large number of hybrid AP systems had been constructed to successfully realize the HER or CRR. Various strategies for system construction were developed, and an obvious improvement of the photocatalytic efficiency of solar fuel production was witnessed, especially in comparison to that of the homogeneous systems using analogous molecular catalysts.[36–38] After ten-years of development, it is time to provide a comprehensive review in this field. In this review, we focus on the development and advances of hybrid AP systems acquired in the last decade. In the above Section 1, an introduction to artificial photosynthesis is given. In Section 2, the mechanism, composition, and strategies for the system design of hybrid AP systems are discussed. The hybrid AP systems for the HER and CRR are reviewed in Section 3 and 4, respectively. The challenges and outlook of this field are given in Section 5.

$2H^+ + 2e^- \longrightarrow H_2$ -0.41 V (1)

$CO_2 + 1e^- \longrightarrow CO_2^{\bullet-}$ -1.90 V (2)

$CO_2 + 2H^+ + 2e^- \longrightarrow HCOOH$ -0.61 V (3)

$CO_2 + 2H^+ + 2e^- \longrightarrow CO + H_2O$ -0.53 V (4)

$2CO_2 + 2H^+ + 2e^- \longrightarrow H_2C_2O_4$ -0.49 V (5)

$CO_2 + 4H^+ + 4e^- \longrightarrow HCHO + H_2O$ -0.48 V (6)

$CO_2 + 6H^+ + 6e^- \longrightarrow CH_3OH + H_2O$ -0.38 V (7)

$CO_2 + 8H^+ + 8e^- \longrightarrow CH_4 + 2H_2O$ -0.24 V (8)

Scheme 2 Electrochemical reaction equations (all potentials *vs.* NHE at pH 7).

2. Hybrid artificial photosynthetic systems

2.1 Mechanism

At present, two terms, photosynthesis and photocatalysis, have not been differentiated in most of the literature. However, it should be noted that from a thermodynamic point of view, an artificial photosynthetic system performs a thermodynamically unfavorable ($\Delta G > 0$) reaction, such as water splitting, with the aid of solar energy input. The photocatalysis is a thermodynamically favorable ($\Delta G < 0$) process.[45–47] Most of the AP systems carry out in the presence of an SED. The thermodynamics of the overall reaction of such systems should be noticed. If the overall reaction is thermodynamically favorable, it is suggested to be referred to as a photocatalytic system. In this review, the term artificial photosynthesis was used to indicate the system mimicking the mechanism of photosynthesis.

The mechanism of the hybrid AP system is depicted in Scheme 3. By using a typical AP system containing three components, a QD, a MC, and a SED, as an example, there are four steps in a complete photocatalytic cycle: (i) light absorption of QDs, (ii) photoinduced electron transfer (PET) between the

QDs and MC, (iii) reduction reaction of the MC for the production of products, and (iv) oxidation reaction of the SED. First, the QDs are excited *via* absorbing visible light to generate electrons and holes in the conduction band (CB) and valence band (VB) of the QDs, respectively (step i in Scheme 3). The photon energy of the light should be higher than the excitation energy (E_a) of the QDs. Second, the photogenerated electrons transfer from the CB of the QDs to the metal center of the MC (step ii in Scheme 3). This is the PET step, one of the most important steps in AP systems.[48–51] The reduced catalyst as an active species binds to the substrate, proton for the HER or CO_2 for the CRR, to fulfill catalytic conversion and finally affords reduction products (step iii in Scheme 3). At the same time, holes in the VB of the QDs are consumed by the SED *via* SED oxidation reactions (step iv in Scheme 3). In a hybrid system, QDs act as a photosensitizer to harvest light and generate electrons of higher potential. A small portion of the HER or CRR may operate at the surface of the QDs; however, the molecular catalyst is the major catalytic center for the catalytic reactions. The conduction band of the QDs should be more negative than the reduction potential of the MC to ensure thermodynamic feasibility of the PET step. Another important parameter is the lifetime of the photogenerated electrons in QDs, and a longer lifetime is kinetically beneficial for PET. However, charge recombination and electron trapping by surface trapping in QDs may decrease the total quantum yield of the system. The kinetic feature of the photogenerated hole consumption is also essential for the stability of the system, and slurry reactions between the SED and holes in QDs lead to self-photocorrosion of the QDs by accumulated holes.

2.2 Photosensitizers

Colloidal quantum dots (QDs) are a kind of photoluminescent material explored in the 1980s.[52,53] Typical QDs are quasi-zero-dimensional materials with a diameter of several nanometers (Table 1). A typical semiconductor QD is composed of a semiconductor core and organic surface ligands (Scheme 4). The presence of organic ligands at the surface causes monodispersion of QDs in solvent. This feature makes QDs have solution processability. QDs as a photosensitizer in a hybrid AP system have the following advantages: (i) the optical properties of QDs can be readily tuned by controlling their size, benefiting from the quantum confinement effect of QDs. The large absorption coefficients and tunable absorption spectra make QDs an excellent light-harvester. (ii) QDs generate multiple excitons under irradiation, which enhance the photon utilization and catalytic efficiency of the hybrid AP system. (iii) The potential of the conduction bond of QDs is negative enough, resulting in QDs to generate excited electrons of more reducing ability. (iv) In comparison to noble metal complexes and organic dyes used as PSs in homogeneous systems, QDs have higher photostability, easier synthetic protocol, and lower cost. (v) QDs can be chemically modified on their surface, and this character expands the process of functionalization of QDs. However, some drawbacks of QDs should also be pointed out. The photocorrosion of QDs caused by hole accumulation in photocatalysis is one of main reasons of system inactivation. Most of the QDs used in AP systems contain cadmium, which is considered to be harmful to the environment.

Colloidal II–VI (CdTe, CdSe, CdS, ZnS, and ZnSe), I–III–VI ($CuInS_2$) QDs and their composites are commonly used as PSs in the hybrid AP systems. The parameters of QDs used in the hybrid AP systems are summarized in Table 1. Most of the QDs are nanoparticles with a diameter in the range of 1–5 nm. The surface of these QDs is passivated by organic ligands containing thiol groups as a surface anchor (Scheme 4).

Carbon-based materials, such as carbon quantum dots (CQDs), are emerging photoluminescent nanoparticles with a diameter from several to hundred nanometers.[54–58] They are synthesized *via* thermolysis by using small organic molecules, such as citric acid and thiophene, as carbon sources. Their surface is terminated by charged groups, such as carboxylic acid and amino, which enable them to disperse evenly in water. Photoluminescent carbon-based nanoparticles are also referred to as carbon quantum dots due to some similarities to inorganic semiconductor quantum dots in terms of photoluminescence and size. Although the chemical structures and the mechanism of photoluminescence of CQDs are controversial, they have been applied in the research of fluorescent sensors, bioimaging, photodynamic therapy, and so on.

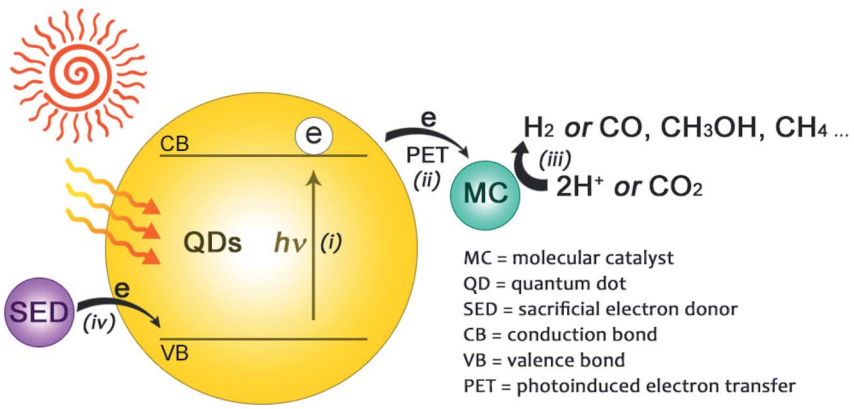

Scheme 3 Mechanism of the hybrid AP system.

Table 1 Physical properties of the QDs used in the hybrid AP systems

Entry	QDs	Ligand	Size/nm	Emission λ_{max}/nm	E_g[a]/eV	Ref.
1	CdTe	**L1**	3.4	625	1.84	44
2	CdTe	**L1**	2.8	557	2.23	104
3	CdTe	**L1**	3.8	N. R.	N. R.	129
4	CdTe	**L11**	2.7	515	2.4	98
5	CdSe	**L1**	1.8	N. R.[b]	2.64	77
6	CdSe	**L1**	N. R.	468	2.64	78
7	CdSe	**L1**	2	N. R.	N. R.	91
8	CdSe	**L1**	N. R.	N. R.	2.19	94
9	CdSe	**L1**	1.95	650	2.7	95
10	CdSe	**L1**	1.9	465	2.7	99
11	CdSe	**L2**	2.5–2.7	N. R.	N. R.	83
12	CdSe	**L2**	2.5–5.5	N. R.	N. R.	80
13	CdSe	**L3**	2.5–2.7	N. R.	2.4	81
14	CdSe	**L4**	2.5–2.7	N. R.	2.4	81
15	CdSe	**L5**	2.2	540	2.13	101
16	CdSe	**L6**	2	474	2.6	102
17	CdSe	**L7**	3	557	2.09	103
18	CdSe	**L9**	2.89–3.63	N. R.	N. R.	106
19	CdS	—[c]	50	N. R.	N. R.	86
20	CdS	—	N. R.	N. R.	N. R.	89
21	CdS	—	N. R.	N. R.	N. R.	90
22	CdS	—	N. R.	N. R.	N. R.	130
23	CdS	—	10	N. R.	N. R.	124
24	CdS	—	5–8	N. R.	2.42	131
25	CdS	—	5.3	451	2.74	125
26	CdS	**L1**	5	630	N. R.	88
27	CdS	**L1**	7.1	610	2.54	123
28	CdS	**L8**	50	N. R.	N. R.	105
29	CdS	**L10**	N. R.	N. R.	2.59	120
30	ZnS	—	50	357	N. R.	87
31	ZnSe	—	3.5–6	N. R.	2.7	126
32	$CuInS_2$	**L1**	6–8	750	N. R.	128
33	$(AgIn)_{0.5}ZnS_2$	—	2.3–4.1	N. R.	2.34	93
34	$Zn_xCd_{1-x}S$	—	N. R.	N. R.	2.46	121
35	$(CuGa)_{1-x}Zn_{2x}S$ ($x = 0.7$)	—	N. R.	N. R.	2.36	127
36	CdSe/ZnS	—	N. R.	540	2.27	96
37	CdS/Bi_2S_3	**L10**	N. R.	N. R.	2.44	119
38	CdS/rGO	—	3.5	N. R.	2.33	113
39	$CuInS_2$/ZnS	—	2.7–3.5	620	N. R.	97
40	$CuInS_2$/ZnS	**L1**	2.5	610	N. R.	118
41	$CuInS_2$/ZnS	**L9**	1.9–2.5	638	1.55	92
42	$CuInS_2$/ZnS	**L12**	2.5	610	N. R.	117
43	CQDs/$ZnIn_2S_4$	—	N. R.	N. R.	N. R.	114
44	CQDs	—	N. R.	N. R.	N. R.	115
45	CQDs	—	20–60	548	2.49	112
46	CQDs	—	4.5–9.1	464	N. R.	108
47	CQDs	—	7	N. R.	N. R.	109
48	N-CQDs[d]	—	<20	N. R.	3.14	111
49	N-CQDs	—	2–4.2	N. R.	N. R.	110
50	CQDs/g-C_3N_4	—	2.3	N. R.	N. R.	122

[a] E_g is the excitation energy of the QDs. [b] N. R. = not recorded. [c] No ligand existing. [d] N-CQDs: Nitrogen-doped carbon quantum dots.

Recently, CQDs have also been used as a photosensitizer to construct hybrid AP systems.

2.3 Catalysts

There are four advantages of using molecular catalysts in hybrid AP systems. (i) Molecular catalysts have a definite chemical structure and are atom economic. (ii) The activity, selectivity, and solubility of molecular catalysts can be tuned through rational ligand design. (iii) Molecular catalysts are easily attached on the surface of QDs physically, chemically, or by self-assembly to form composite photocatalysts. (iv) Molecular catalysts are good models for the mechanism study. Transition metal (Fe, Co, and Ni) complexes are major molecular catalysts used in hybrid AP systems (Schemes 5–8, Table 2).[59–62] The HER molecular catalysts include hydrogenase mimics, cobaloxime and its derivatives, Ni-bis(diphosphine) complexes, and so on (Schemes 5–7).

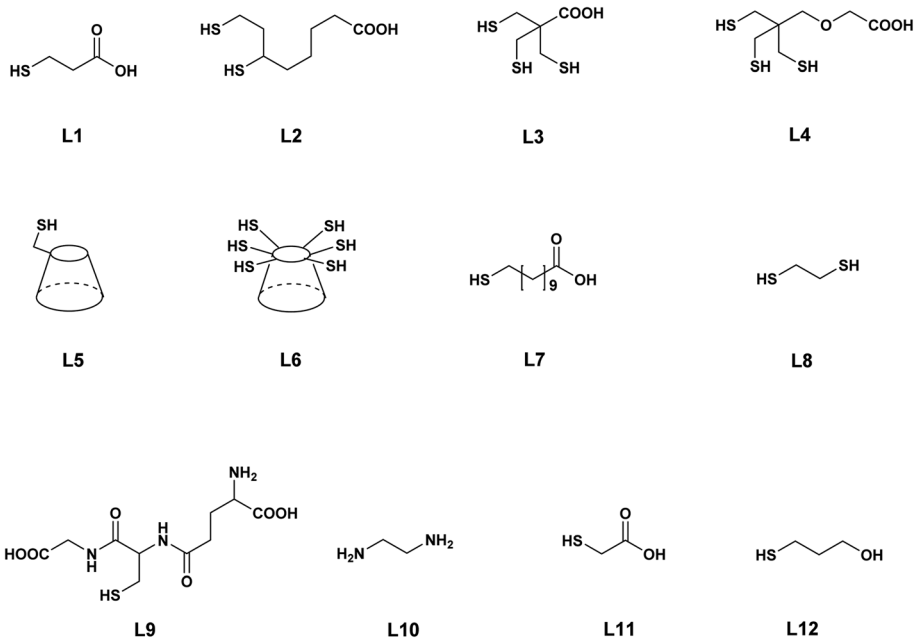

Scheme 4 Chemical structures of the QD ligands.

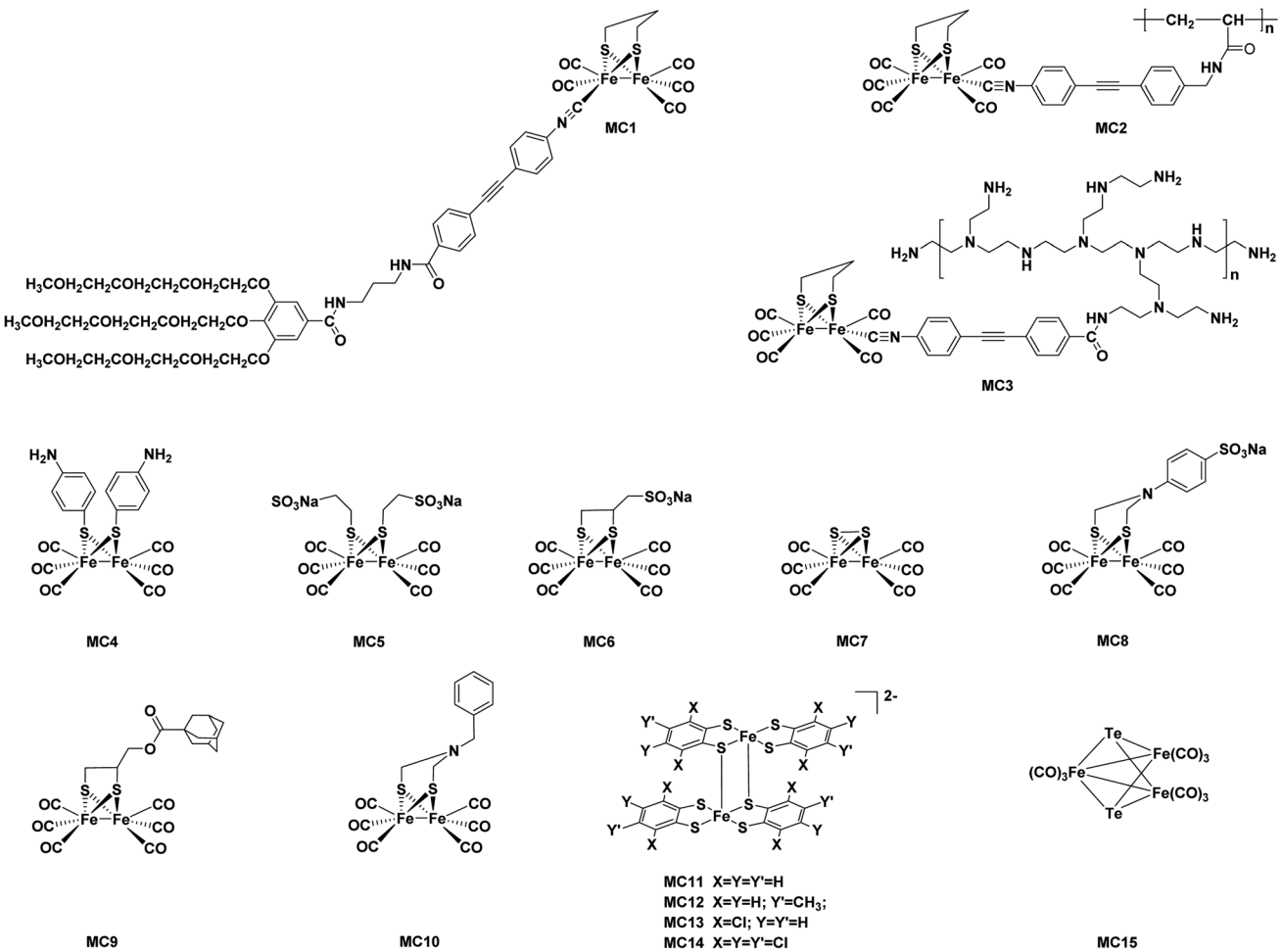

Scheme 5 Chemical structures of the Fe-based molecular catalysts for the HER.

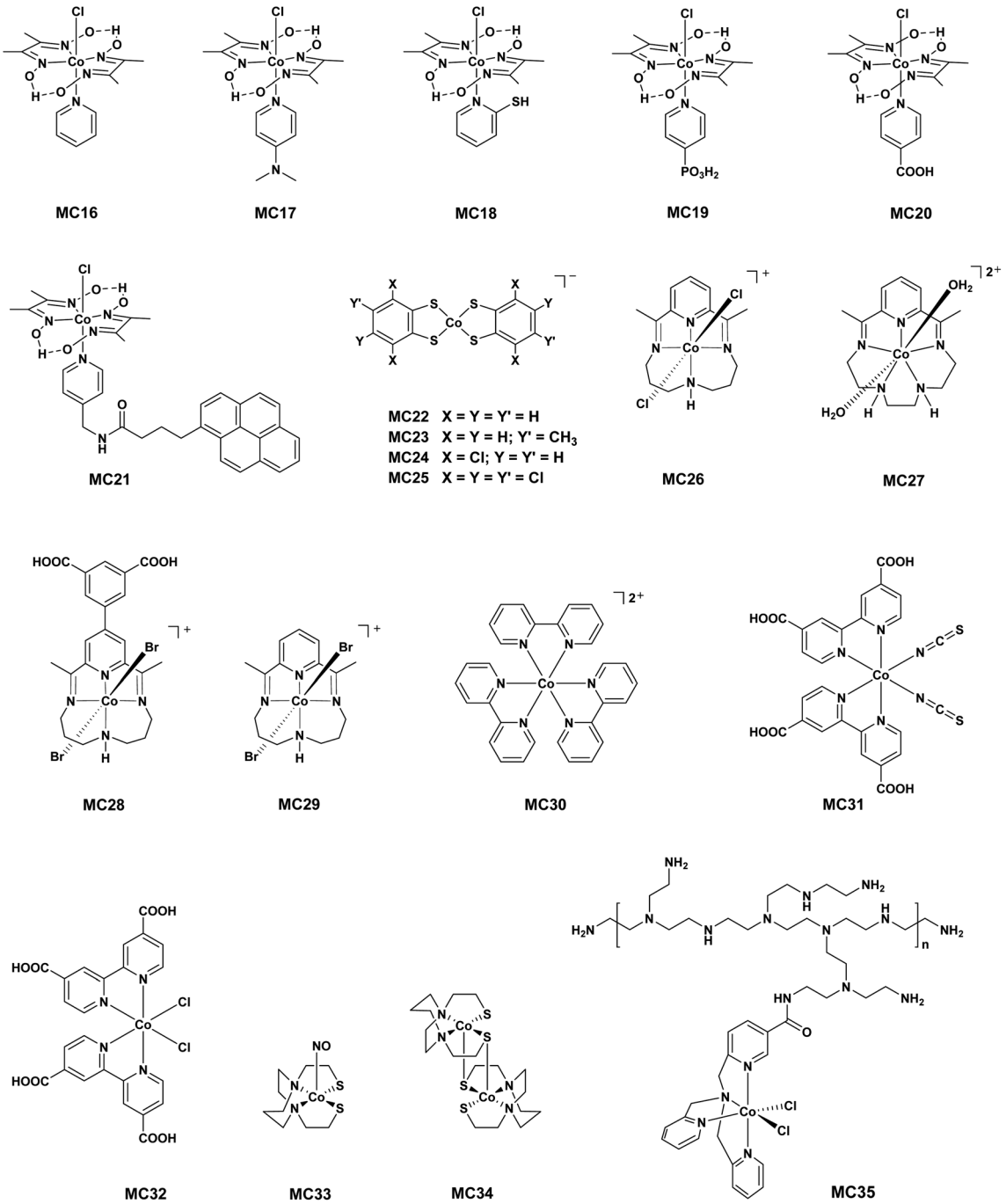

Scheme 6 Chemical structures of the Co-based molecular catalysts for the HER.

Hydrogenase mimics are complexes containing an Fe_2S_2 core. They are named hydrogenase mimics because the structure of Fe_2S_2 is similar to the active site of [FeFe]-hydrogenase in algae, and the latter catalyzes a reversible proton reduction reaction with an exceptional activity.[63] It should be noted that the Fe_2S_2-based mimics are based on an Fe^IFe^I diiron core, which is different from the natural active site of an $Fe^{II}Fe^{II}$ core. The Fe^IFe^I mimics had been proved to have catalytic activity for proton reduction in either photocatalytic or electrocatalytic systems. The active species is a one-electron reduced Fe^IFe^0 species, which binds to a proton to form a hydride intermediate for affording H_2. The Fe_2S_2 mimics can be modified and functionalized at either Fe atoms or S atoms. Given this advantage, various hydrogenase mimics (Scheme 5) were synthesized for the construction of AP systems. Early this century, many Fe_2S_2 complexes were used as molecular catalysts in combination with a molecular PS covalently or intermolecularly, such as $[Ru(bpy)_3]^{2+}$, zinc-porphyrins, and organic dyes, for homogeneous photocatalytic H_2 production. However, most of these systems produced H_2 with a TON (all TONs are based on

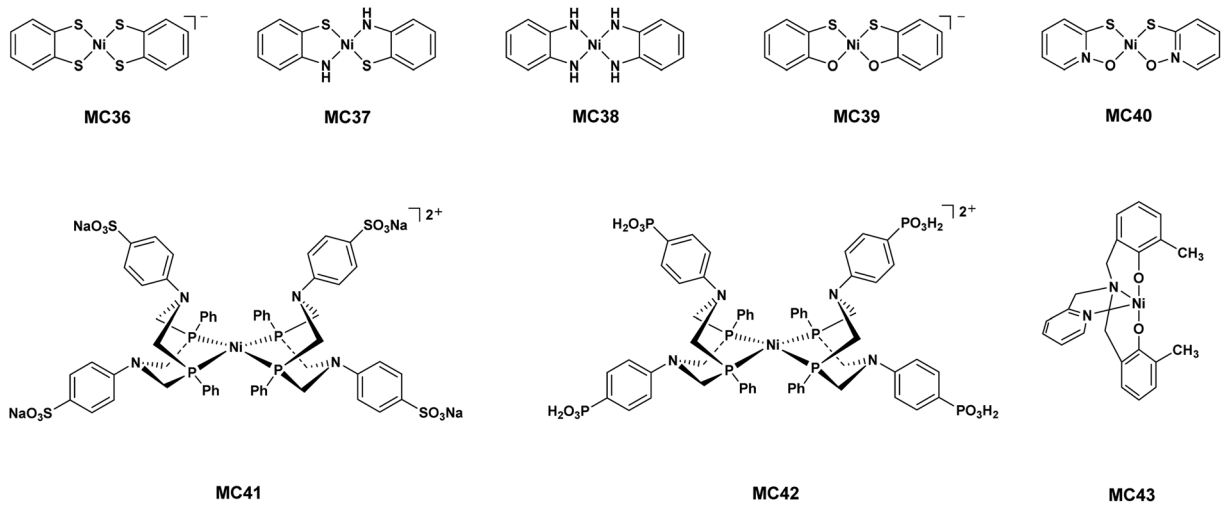

Scheme 7 Chemical structures of the Ni-based molecular catalysts for the HER.

molecular catalysts in this review) of no more than 1 to several turnovers.[48]

Cobaloxime had long been known as a molecular catalyst for the HER.[64,65] The catalytic mechanism of cobaloxime for the HER had been studied extensively. A two-electron reduced Co^{I}-species is the active species for proton binding. Cobaloxime can be functionalized at the axial pyridine ligand, and this facilitates chemists to develop various cobaloxime

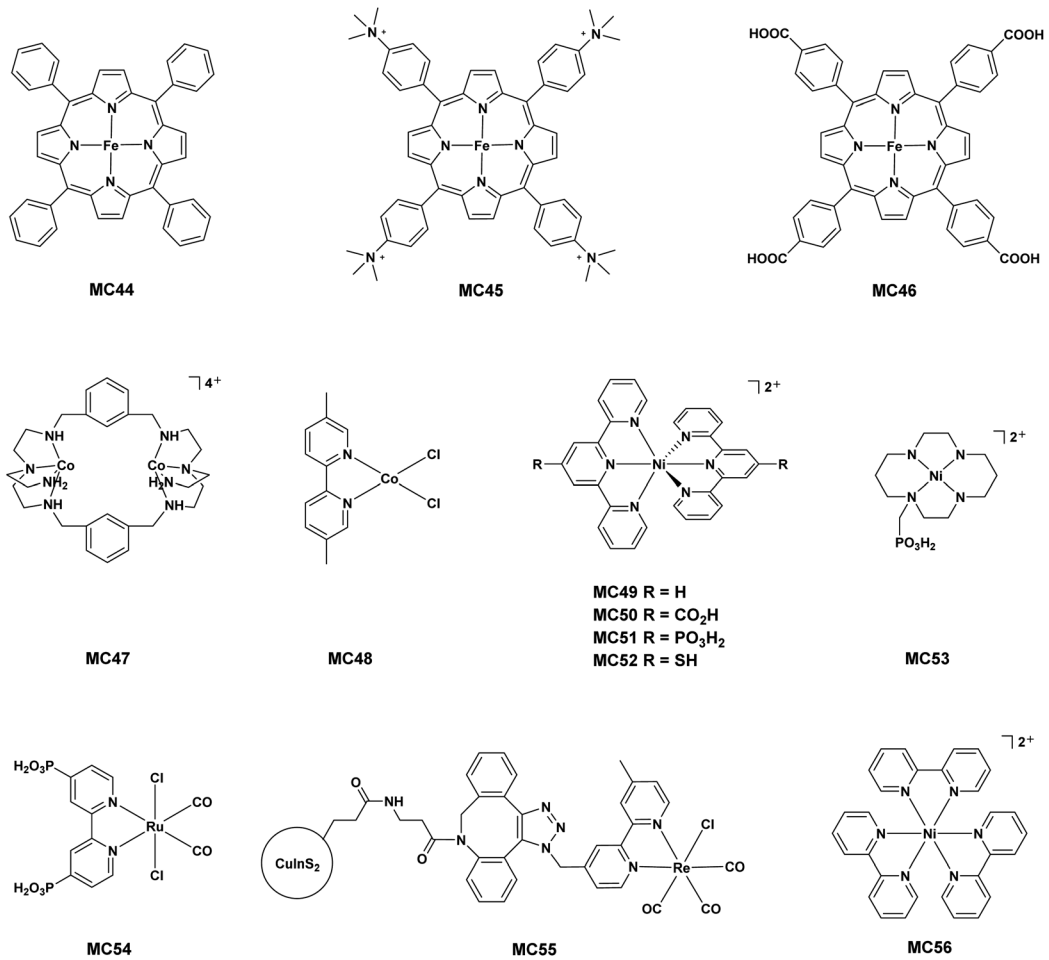

Scheme 8 Chemical structures of the molecular catalysts for the CRR.

Table 2 Reductive potentials of the MCs used in the hybrid AP systems

Entry	MC	Reduction couples	E_{red}/eV	*vs.* RE	Solvent	Ref.
1	**MC1**	$Fe^{I}Fe^{I}/Fe^{I}Fe^{0}$	−0.88	NHE	CH_3CN	44
2	**MC2**	$Fe^{I}Fe^{I}/Fe^{I}Fe^{0}$	−0.43	NHE	CH_3CN	77
3	**MC3**	$Fe^{I}Fe^{I}/Fe^{I}Fe^{0}$	−0.55	NHE	CH_3CN	78
4	**MC4**	$Fe^{I}Fe^{I}/Fe^{I}Fe^{0}$	−1.07	NHE	DMF	87
5	**MC5**	$Fe^{I}Fe^{I}/Fe^{I}Fe^{0}$	−0.90	NHE	CH_3CN	91
6	**MC6**	$Fe^{I}Fe^{I}/Fe^{I}Fe^{0}$	−1.05	NHE	CH_3CN	91
7	**MC7**	$Fe^{I}Fe^{I}/Fe^{I}Fe^{0}$	−0.66	NHE	CH_3CN	99
8	**MC8**	$Fe^{I}Fe^{I}/Fe^{I}Fe^{0}$	−0.97	NHE	H_2O	101
9	**MC9**	$Fe^{I}Fe^{I}/Fe^{I}Fe^{0}$[a]	−1.13	NHE	H_2O/IPA	102
10	**MC9**	$Fe^{I}Fe^{I}/Fe^{I}Fe^{0}$	−1.09	NHE	H_2O/IPA	102
11	**MC9**	$Fe^{I}Fe^{I}/Fe^{I}Fe^{0}$	−0.96	NHE	CH_3CN	102
12	**MC10**	$Fe^{I}Fe^{I}/Fe^{I}Fe^{0}$	−1.16	NHE	CH_3OH/H_2O	104
13	**MC11**	$Fe^{II/I}$	−0.928	SCE	CH_3CN	83
14	**MC12**	$Fe^{II/I}$	−0.898	SCE	CH_3CN	83
15	**MC13**	$Fe^{II/I}$	−0.764	SCE	CH_3CN	83
16	**MC14**	$Fe^{II/I}$	−0.723	SCE	CH_3CN	83
17	**MC15**	N. R.	−1.38	NHE	N. R.	95
18	**MC16**	$Co^{III/II}$, $Co^{II/I}$	−0.35, −0.78	NHE	DMF	86
19	**MC17**	$Co^{III/II}$, $Co^{II/I}$	−0.44, −0.79	NHE	DMF	86
20	**MC18**	$Co^{III/II}$, $Co^{II/I}$	−0.48, −0.80	NHE	DMF	86
21	**MC16**	$Co^{III/II}$, $Co^{II/I}$	−0.36, −0.79	NHE	DMF	88
22	**MC16**	$Co^{III/II}$, $Co^{II/I}$	−0.41, −0.85	NHE	H_2O	89
23	**MC16**	$Co^{III/II}$, $Co^{II/I}$	−0.35, −0.78	NHE	CH_3CN	114
24	**MC19**	$Co^{III/II}$, $Co^{II/I}$	−0.77, −1.08	SCE	DMF	96
25	**MC20**	$Co^{II/I}$	−0.47	NHE	H_2O	116
26	**MC21**	$Co^{III/II}$, $Co^{II/I}$	−0.24, −0.82	NHE	CH_3CN	113
27	**MC22**	$Co^{II/I}$	−0.70	SCE	CH_3CN/H_2O	81
28	**MC23**	$Co^{II/I}$	−0.64	SCE	CH_3CN/H_2O	81
29	**MC24**	$Co^{II/I}$	−0.51	SCE	CH_3CN/H_2O	81
30	**MC25**	$Co^{II/I}$	−0.40	SCE	CH_3CN/H_2O	81
31	**MC26**	$Co^{II/I}$	−0.85	SCE	N. R.	92
32	**MC27**	$Co^{II/I}$	−1.03	SCE	N. R.	92
33	**MC26**	$Co^{II/I}$	−0.61	NHE	H_2O	111
34	**MC28**	$Co^{II/I}$	−0.68	NHE	H_2O	97
35	**MC29**	$Co^{II/I}$	−0.68	NHE	H_2O	97
36	**MC30**	$Co^{II/I}$	−0.95	NHE	N. R.	93
37	**MC33**	$Co^{II/I}$	−1.08	NHE	CH_3CN	98
38	**MC34**	$Co^{II/I}$	−0.85	NHE	CH_3CN	98
39	**MC35**	$Co^{II/I}$	−1.47	NHE	H_2O	112
40	**MC36**	$Ni^{II/I}$	−0.56	SCE	CH_3CN	82
41	**MC37**	$Ni^{II/I}$	−0.11	SCE	CH_3CN	82
42	**MC38**	$Ni^{II/I}$	−0.89	SCE	CH_3CN	82
43	**MC39**	$Ni^{II/I}$	−0.45	SCE	DMF	82
44	**MC40**	$Ni^{II/I}$	−1.32	SCE	CH_3CN	82
45	**MC41**	$Ni^{II/I}$	−0.558	SCE	H_2O	94
46	**MC43**	$Ni^{II/I}$	−0.95	NHE	CH_3CN	103
47	**Ni^{2+}-DHLA**[b]	$Ni^{II/I}$	−0.90	NHE	$EtOH/H_2O$	80
48	**Ni^{2+}-EDT**[b]	$Ni^{II/I}$	−0.11	RHE	H_2O	105
49	**Co^{2+}-GSH**[b]	$Co^{II/I}$	−0.70	NHE	H_2O	106
50	**MC45**	$Fe^{I/0}$	−1.80	SCE	DMF	118
51	**MC46**	$Fe^{I/0}$	−1.02	NHE	N. R.	119
52	**MC46**	$Fe^{I/0}$	−1.02	NHE	DMF	120
53	**MC46**	$Fe^{I/0}$	−1.02	NHE	DMF	121
54	**MC46**	$Fe^{I/0}$	−1.02	NHE	DMF	122
55	**MC47**	$Co^{II/I}$	−0.80	NHE	H_2O	123
56	**MC49**	$Ni^{II/I}$	−1.58	Fc/Fc^{+}	CH_3CN/H_2O	124
57	**MC50**	$Ni^{II/I}$	−1.70	Fc/Fc^{+}	CH_3CN/H_2O	125
58	**MC53**	$Ni^{II/I}$	−1.0	NHE	N. R.	126
59	**MC55**	$Re^{I/0}$	−0.93	SCE	DMSO	128

[a] In the presence of β-cyclodextrin. [b] Active sites formed by metal ions and the ligand in the QDs.

derivatives for anchoring or other functions of the catalyst. However, the axial pyridine ligand readily dissociates upon reduction, and this should be noticed by researchers in system construction and mechanism studies.[66] Eisenberg successfully realized homogeneous photocatalytic H_2 production by using cobaloxime and the derivatives as catalysts in combination with molecular PSs, such as organic dyes and Pt-complexes. The H_2 production activity and stability of these systems are limited, and the H_2 production TON is 55.8 and 181.5 for systems containing a Pt-complex and Eosin Y, respectively.[67–69]

The Ni-bis(diphosphine) complex is also known as the DuBois catalyst or mimic of hydrogenase.[70] In 2011, DuBois *et al.* reported a Ni^{II}-complex supported by two bis(diphosphine) ligands having exceptional activity for electrocatalytic H_2 production. The complex features four nitrogen atoms as proton relays surrounding the nickel center. This is similar to the function of a –NH– group near the iron center in the active site of hydrogenase. In the same year, Eisenberg and Holland *et al.* reported that the Dubois catalyst in combination with a molecular PS, $Ru(bpy)_3]^{2+}$ or eosin Y, in a water/acetonitrile mixed solution produced H_2 under visible light irradiation. A TON of 2700 after 150 hours of photocatalysis was obtained by using $Ru(bpy)_3]^{2+}$ as a PS.[71] In addition to these three types of HER molecular catalysts, cobalt complexes of N_2S_2 ligands and polypyridyl ligands and nickel complexes of S_4, N_2S_2, and S_2O_2 ligands were explored as HER molecular catalysts for constructing hybrid AP systems.

The metal complexes used as CRR catalysts in hybrid AP systems are tetraphenylporphyrin iron(III) chloride and its derivatives, dinulcear and mononuclear cobalt complexes, nickel cyclam and $[Ni(tpy)_2]^{2+}$ complexes, and Re^{I} and Ru^{II} complexes (Scheme 8).[72–74] The Fe^{III}-tetraphenylporphyrins are efficient CRR catalysts used in homogeneous electrochemical or photochemical CRR systems. The two-electron reduced Fe^{0}-species is the active site for CO_2 binding. The Co^{II} and Ni^{II} complexes supported by ligands of tetra- or hexa-nitrogen atoms are active towards CO_2 in their metal-centered one-electron reduced Co^{I} and Ni^{I} states. Carbonyl Re^{I} and Ru^{II} complexes are also active towards CO_2 in Re^{0} and Ru^{I} states.

2.4 Sacrificial electron donors

The sacrificial electron donors used in hybrid AP systems are small organic molecules that are easily oxidized (Scheme 9).[75,76] Organic acids and their salts (ascorbic acid or sodium ascorbate), amines (triethylamine and triethanolamine), alcohols (isopropyl alcohol), sulphides (Na_2S) and sulphites (Na_2SO_3) are the most commonly used electron donors. The oxidation potential of SEDs and the valence band potential of QDs should match thermodynamically. The solubility of the electron donors in solvent also quite affects the efficiency of the system. To achieve fast removal of holes from QDs, electron donors in the system should have a good solubility and a high concentration. Ascorbic acid (AA), IPA, TEOA, Na_2S and Na_2SO_3 are soluble in water and can be used in aqueous systems. AA, Na_2S, and Na_2SO_3 are poorly soluble in organic solvents, and TEA is poorly soluble in water. IPA and TEOA can be used in either water or most commonly used organic solvents.

2.5 Solvents

Solvent is the medium and environment for AP reactions. Most of the hybrid AP systems for the HER were constructed in aqueous solution due to kinetically favorable proton reduction in water (Table 3). The concentration of protons can be controlled easily by adjusting the pH of the solution. In contrast, most of the hybrid AP systems for the CRR were constructed in organic solvents or a mixture of organic solvent and water. There are two reasons. First, the solubility of CO_2 is

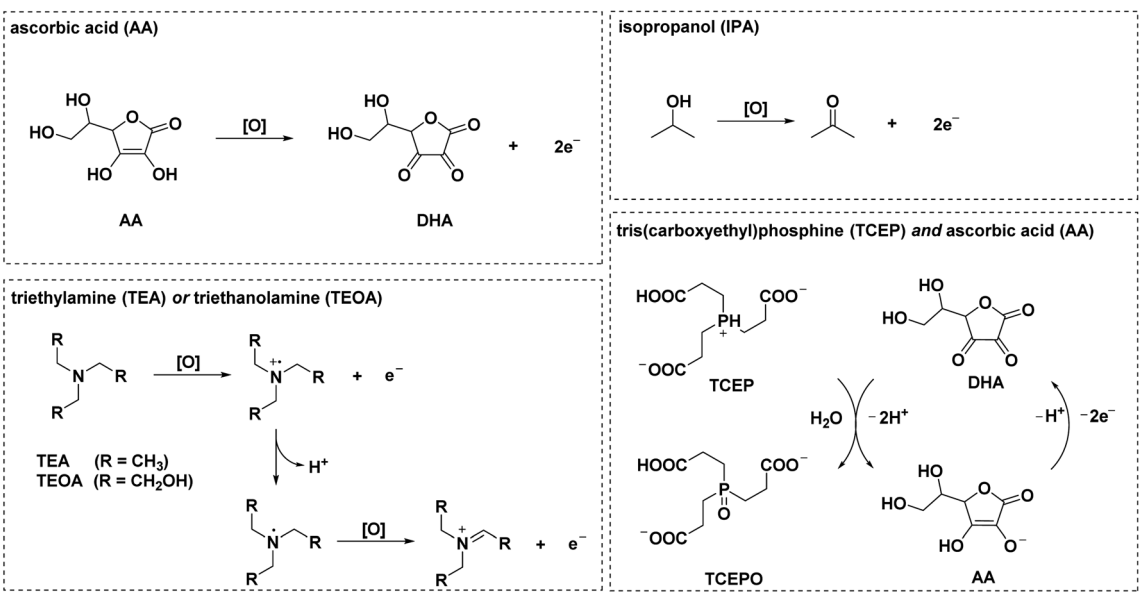

Scheme 9 Oxidation reactions of the organic molecules used as SEDs.

Table 3 Components, conditions, and photocatalytic efficiencies of the hybrid AP systems for the HER

Entry	PS	MC	SED	Solvent	pH	Light source[a]	Irradiation time/h	TON[b]	QY[c]/%	Ref.
1	MPA-CdTe	**MC1**	AA	H_2O	4.0–4.1	Xe ($\lambda > 400$ nm)	10	505	45.8 (365 nm)	44
2	MPA-CdSe	**MC2**	AA	H_2O	4.0	LED ($\lambda = 450$ nm)	8	27 135	5.07 (450 nm)	77
3	MPA-CdSe	**MC3**	AA	H_2O	6.5	LED ($\lambda = 410$ nm)	44	10 600	2.1 (470 nm)	78
4	ZnS	**MC4**	AA	DMF/H_2O	4.6	Xe	38	2607	2.5 (325 nm) **	87
5	MPA-CdSe	**MC5**	AA	H_2O	4	LED ($\lambda = 450$ nm)	12	26 500	N. R.	91
6	MPA-CdSe	**MC6**	AA	H_2O	4	LED ($\lambda = 450$ nm)	12	18 800	N. R.	91
7	MPA-CdSe	**MC7**	AA	H_2O	4.0	LED ($\lambda = 410$ nm)	82	8781	N. R.	99
8	**L5**-CdSe	**MC8**	AA	H_2O	4.5	Xe ($\lambda > 400$ nm)	28	2370	3.19 (400 nm)**	101
9	**L6**-CdSe	**MC9**	IPA	H_2O	8.0	LED ($\lambda = 410$ nm)	48	11 200	N. R.	102
10	MPA-CdTe	**MC10**	AA	CH_3OH/H_2O	4.5	LED ($\lambda = 410$ nm)	60	52 800	38.3 (575 nm)	103
11	DHLA-CdSe	**MC11**	AA	EtOH/H_2O	4.5	LED ($\lambda = 520$ nm)	80	20 600	N. R.	83
12	DHLA-CdSe	**MC12**	AA	EtOH/H_2O	4.5	LED ($\lambda = 520$ nm)	80	29 400	N. R.	83
13	DHLA-CdSe	**MC13**	AA	EtOH/H_2O	4.5	LED ($\lambda = 520$ nm)	80	15 200	N. R.	83
14	DHLA-CdSe	**MC14**	AA	EtOH/H_2O	4.5	LED ($\lambda = 520$ nm)	80	8000	N. R.	83
15	MPA-CdSe	**MC15**	AA	H_2O	4	Xe ($\lambda > 400$ nm)	8	2820*	N. R.	95
16	CdS	**MC16**	TEOA	CH_3CN/H_2O	7	Xe ($\lambda > 420$ nm)	15	171	9.1 (420 nm)	86
17	CdS	**MC17**	TEOA	DMF/H_2O	7	Xe ($\lambda > 420$ nm)	N. R.	N. R.	N. R.	86
18	CdS	**MC18**	TEOA	DMF/H_2O	7	Xe ($\lambda > 420$ nm)	N. R.	N. R.	N. R.	86
19	MPA-CdS	**MC16**	N. R.	N. R.	N. R.	N. R.	N. R.	N. R.	N. R.	88
20	CdS	**MC16**	CH_3OH	H_2O	13.5	Xe ($\lambda \geq 420$ nm)	4	36*	N. R.	89
21	CdS	**MC16**	CH_3OH	H_2O	4	Xe ($\lambda \geq 420$ nm)	N. R.	N. R.	N. R.	90
22	CQDs/$ZnIn_2S_4$	**MC16**	TEOA	H_2O	7	Xe ($\lambda > 420$ nm)	8	567*	N. R.	114
23	CdSe/ZnS	**MC19**	TEOA	H_2O	N. R.	Xe ($\lambda > 400$ nm)	10	>10 000[d]	N. R.	96
24	CdS nanorod	**MC20**	Lactic acid	H_2O	2.4	Xe ($\lambda \geq 420$ nm)	200	2000*	N. R.	116
25	CdS/rGO	**MC21**	Na_2S/Na_2SO_3	DMF/H_2O	13.3	LED ($\lambda = 450$ nm)	80	22 464	N. R.	113
26	**L4**-CdSe	**MC22**	AA	H_2O	4.5	LED ($\lambda = 520$ nm)	60	>300 000	24 (520 nm)	81
27	**L3**-CdSe	**MC23**	AA	H_2O	4.5	LED ($\lambda = 520$ nm)	46	55 238	N. R.	81
28	**L3**-CdSe	**MC24**	AA	H_2O	4.5	LED ($\lambda = 520$ nm)	46	26 815	N. R.	81
29	**L3**-CdSe	**MC25**	AA	H_2O	4.5	LED ($\lambda = 520$ nm)	46	14 375	N. R.	81
30	GSH-$CuInS_2$/ZnS	**MC26**	NaHA/AA	H_2O	5.0	Xe ($\lambda > 400$ nm)	96	7700	N. R.	92
31	GSH-$CuInS_2$/ZnS	**MC27**	NaHA/AA	H_2O	5.0	Xe ($\lambda > 400$ nm)	22	180	N. R.	92
32	N-CQDs	**MC26**	TCEP/AA	H_2O	5	LED ($\lambda = 375$ nm)	52	859	26	111
33	$CuInS_2$/ZnS	**MC28**	AA	H_2O	4.5	Xe ($\lambda > 400$ nm)	8	2670	5.84 (420 nm)***	97
34	$CuInS_2$/ZnS	**MC29**	AA	H_2O	4.5	Xe ($\lambda > 400$ nm)	8	1360	2.89 (420 nm)***	97
35	$(AgIn)_{0.5}ZnS_2$	**MC30**	AA	Toluene/EtOH/H_2O	N. R.	Xe ($\lambda > 420$ nm)	12	2420	8.2 (450 nm)**	93
36	CQDs	**MC31**	TEOA	H_2O	N. R.	Xe ($\lambda > 420$ nm)	4	49.9*	14.11 (450 nm)**	115
37	TGA-CdTe	**MC33**	AA	H_2O	5.5	Xe ($\lambda > 400$ nm)	70	23 000	5.32 (400 nm)	88
38	TGA-CdTe	**MC34**	AA	H_2O	5.5	Xe ($\lambda > 400$ nm)	30	4900	1.49 (400 nm)	88
39	CQDs	**MC35**	NaHA	H_2O	8.4	LED ($\lambda = 450$ nm)	36	198	N. R.	112
40	**L3**-CdSe	**MC40**	AA	H_2O	4.5	LED ($\lambda = 520$ nm)	90	>130 000	N. R.	82
41	MPA-CdSe	**MC41**	AA	H_2O	3.8	LED ($\lambda = 505$ nm)	10	511	N. R.	94
42	CQDs	**MC42**	EDTA	H_2O	6	Xe ($\lambda > 300$ nm)	4	64	2.3 (360 nm)***	108
43	CQDs	**MC42**	TCEP/AA	H_2O	6	Xe ($\lambda > 300$ nm)	24	1094	N. R.	109
44	N-CQDs	**MC42**	EDTA	H_2O	6	Xe ($\lambda > 400$ nm)	4	277	N. R.	110
45	MUA-CdSe	**MC43**	AA	H_2O	7	LED ($\lambda = 420$ nm)	3.5	10 667	N. R.	103
46	DHLA-CdSe	**Ni^{2+}-DHLA**	AA	H_2O	4.5	LED ($\lambda = 520$ nm)	360	>600 000	36 ± 10 (520 nm)	80
47	DHLA-CdSe	**Ni^{2+}-DHLA**	AA	EtOH/H_2O	4.5	LED ($\lambda = 520$ nm)	10	34 600	59 (520 nm)***	107
48	DHLA-CdSe/CdS	**Ni^{2+}-DHLA**	AA	EtOH/H_2O	4.5	LED ($\lambda = 520$ nm)	10	3390	13 (520 nm)***	107
49	DHLA-CdSe rods	**Ni^{2+}-DHLA**	AA	EtOH/H_2O	4.5	LED ($\lambda = 520$ nm)	10	7450	5.8 (520 nm)***	107
50	DHLA-CdSe/CdS DIRs[e]	**Ni^{2+}-DHLA**	AA	EtOH/H_2O	4.5	LED ($\lambda = 520$ nm)	10	795	1.4 (520 nm)***	107
51	EDT-CdS	**Ni^{2+}-EDT**	Na_2S/Na_2SO_3	H_2O	N. R.	Xe ($\lambda > 400$ nm)	84	>8000	19.4 (460 nm)	105
52	GSH-CdSe	**Co^{2+}-GSH**	AA	H_2O	4.5	LED ($\lambda = 525$ nm)	48	130 000	28 ± 5 (525 nm)	106

[a] Xe and LED mean Xe lamp and LED lamp. [b] TON is based on the molecular catalyst. *The value is calculated using the given data in the reference. [c] QY = quantum yield; The wavelength in parentheses represents the wavelength used in QY measurements; **Apparent Quantum yield; ***Internal Quantum yield. [d] Based on the QDs. [e] DIR: dot-in-rod structure.

higher in organic solvents (DMF, DMSO, CH_3CN, *etc.*) than that in water. Second, proton reduction is a competing reaction of the CRR, and the former is prone to occur in water. To achieve a higher selectivity and efficiency of the CRR, aprotic organic solvents, such as DMF, DMSO, and CH_3CN, were chosen for the CRR. The development of aqueous AP systems for the CRR with high selectivity and efficiency is a challenge faced by researchers.

2.6 Strategies of system design

Many strategies had been developed to construct hybrid AP systems (Scheme 10). The simplest way is mixing QDs and molecular catalysts physically. The interaction between a PS and MC is intermolecular. Another strategy is covalently linking MCs to QDs or self-assembling MCs on the surface of QDs to form a **MC@QD** type composite photocatalyst. This strategy is expected to improve the efficiency of PET by shortening the distance between QDs and MCs. To this end, various methods, such as covalent linking, host-guest recognition, electrostatic attraction, *etc.*, have been applied. Several **MC@QD** photocatalysts were fabricated by *in situ* formation of molecular-like species on the surface of QDs. To improve catalytic efficiency and develop biomimic systems, the multi-component integration systems of loading QDs and MCs onto functional materials had been reported.

2.7 Catalytic performance parameters

There are several parameters that are commonly used to evaluate the catalytic performance of a hybrid photosynthetic system. The turnover number (TON) is defined as the number of catalytic turnovers of a catalyst in a particular system, which is calculated using eqn (1). The value of the TON reflects the catalytic ability of a catalyst; however, it neither reflects the efficiency of a catalyst nor the efficiency of photon utilization of the system. The turnover number frequency (TOF), calculated using eqn (2), is used to evaluate the catalytic efficiency of a catalyst in a particular system. These two parameters are used in all kinds of catalytic systems. In the studies of hybrid artificial photosynthetic systems, TONs and TOFs are calculated based on molecular catalysts. One can assess the catalytic performance of a particular molecular catalyst in different systems by comparing these two parameters. For a photocatalytic system, the photon utilization efficiency of a system is also an important parameter. The quantum yield (QY) or apparent quantum yield (AQY) is used to assess the conversion efficiency of the photon-to-product of a system. The QY is defined as the ratio of the number of products produced from the system to the number of absorbed photons by the system, which is calculated using eqn (3). Although QYs were reported in most of the studies in this field, it is not suitable to compare QYs reported by different research groups. This is because of the measurement method of photon absorption varying in different groups. The QY value is highly affected by the measurement method and setup. Herein, a standard method of QY measurement in photocatalysis is needed to be established. The photocatalytic CO_2 reduction system always produces H_2 as a by-product and more than one CO_2 reduction product, so selectivity is used to evaluate the specificity for the CRR of a particular system. The selectivity is calculated using eqn (4).

$$\mathrm{TON} = \frac{n_{\mathrm{product}}}{n_{\mathrm{catalyst}}} \quad (1)$$

$$\mathrm{TOF} = \frac{\mathrm{TON}}{t} \quad (2)$$

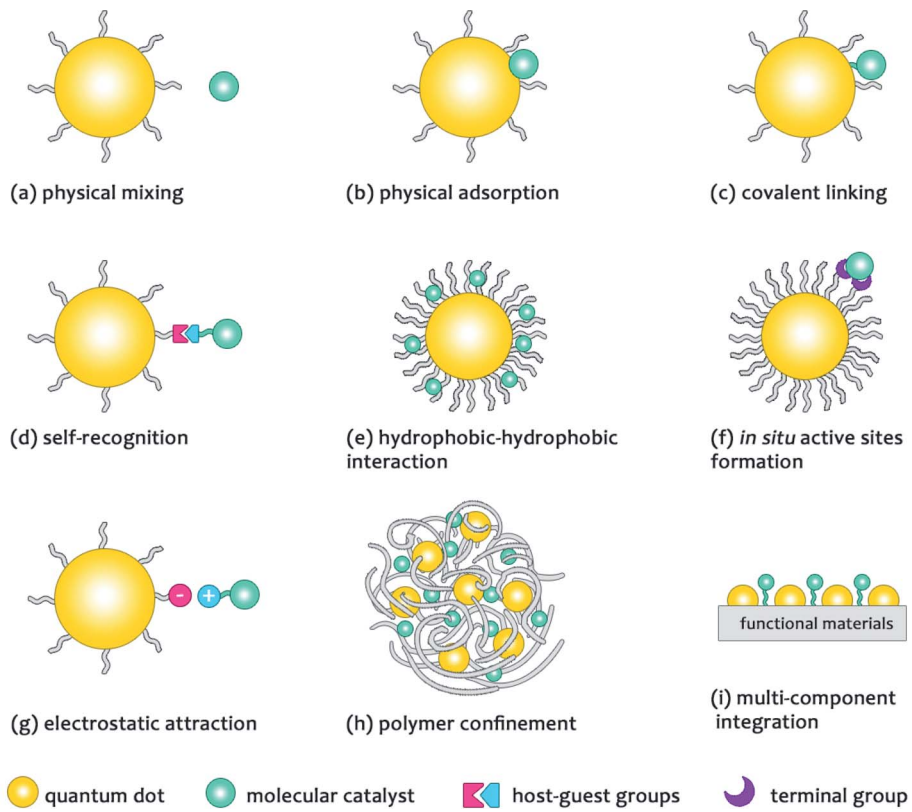

Scheme 10 Schematic diagram of the strategies used for the construction of hybrid AP systems.

$$\mathrm{QY} = \frac{n_{\mathrm{product}}}{n_{\mathrm{photon}}} \quad (3)$$

$$\mathrm{Selectivity} = \frac{n_{\mathrm{product}}}{n_{\mathrm{total\ products}}} \quad (4)$$

3. Hybrid AP systems for the HER

3.1 Physical mixing systems

In 2011, Wu *et al.* used a water soluble [FeFe]-hydrogenase mimic **MC1** as a MC, colloidal MPA-CdTe QDs (MPA = 3-mercaptopropionic acid, **L1**) as a PS, and AA as a SED to construct an aqueous system for photocatalytic H_2 production (Scheme 11).[44] The H_2 production activity and the stability of the system are far higher than those of homogeneous systems reported previously containing molecular photosensitizers and hydrogenase mimics. A TON of 505 was obtained in aqueous solution at pH 4. The PET from the CB of CdTe QDs to the Fe_2S_2 core of **MC1** occurs resulting in the formation of a $Fe^{I}Fe^{0}$ species, which is the active species for proton binding and reduction. This is the first hybrid AP system. Followed by this work, a large number of such hybrid AP systems, namely the combination of molecular catalysts and colloid QDs, were developed.

By grafting Fe_2S_2 active sites onto poly(acrylic acid) (PAA) or polyethylenimine (PEI), two water-soluble polymeric mimics, **MC2** or **MC3**, respectively, were prepared by Wu.[77,78] These two mimics were applied to construct HER systems in combination with MPA-CdSe QDs and AA. The former in acidic aqueous solution produced H_2 with a TON of 27 135.[77] The catalytic activity of the system ceased within 8 hours. In contrast, the latter exhibited high activity and stability in neutral aqueous solution due to buffer properties of PEI, and a TON of 10 600 was obtained by **MC3** at pH 6.5.[78] In another system, the stability of **MC2** could be improved by adding PEI, which forms a secondary coordination sphere around the QDs to accelerate hole transfer from the QDs to AA.[79] Benefiting from the fast H_2 production rate and the improved stability of the system, the TON under such conditions increased to 83 600.

The capping ligands of QDs are usually small hydrophilic molecules of thiol groups, which are easy to dissociate from the surface of QDs in AP system solutions. This results in the aggregation of QDs and may form new catalytic species between dissociated ligands and molecular catalysts. In 2012, Eisenberg *et al.* reported that dihydrolipoic acid (DHLA, **L2**) dissociated from DHLA-CdSe QDs is able to bind to Ni^{2+} and forms active DHLA-Ni^{2+} species for H_2 production (Scheme 12).[80] The photocatalytic system composed of DHLA-CdSe QDs as a PS, $Ni(NO_3)_2$ as a catalyst precursor, and AA as a SED in aqueous solution of pH 4.5 produced H_2 with exceptional activity and stability. A TON exceeding 600 000 and a quantum yield of 36% were obtained. The H_2 production activity was maintained over 360 hours. To prevent ligand dissociation from QDs, they used tripodal S-donor ligand (**L3** and **L4**) capped CdSe QDs as a PS in combination with a series of molecular catalysts based on iron (**MC11–MC14**), cobalt (**MC22–MC25**), and nickel (**MC36–MC40**) for photocatalytic H_2 production in aqueous solutions in their following studies.[81–83] The highest TON of 300 000 was obtained in 60 hours by using **L4**-CdSe QDs as a PS, **MC22** as a catalyst, and AA as a SED, and the QY of H_2 production was 24% with 520 nm light.[81] **MC22** was also investigated by using $[Ru(bpy)_3]^{2+}$ as a PS; however, the activity and stability of the homogeneous system are lower than those of the hybrid system.[84,85] The former produced H_2 with a TON of 2700 and the system is short-lived (<6 h) due to the decomposition of the molecular PS and the catalyst.

Li *et al.* extensively studied the PET process between molecular catalysts (**MC4** and **MC16–MC18**) and nano-

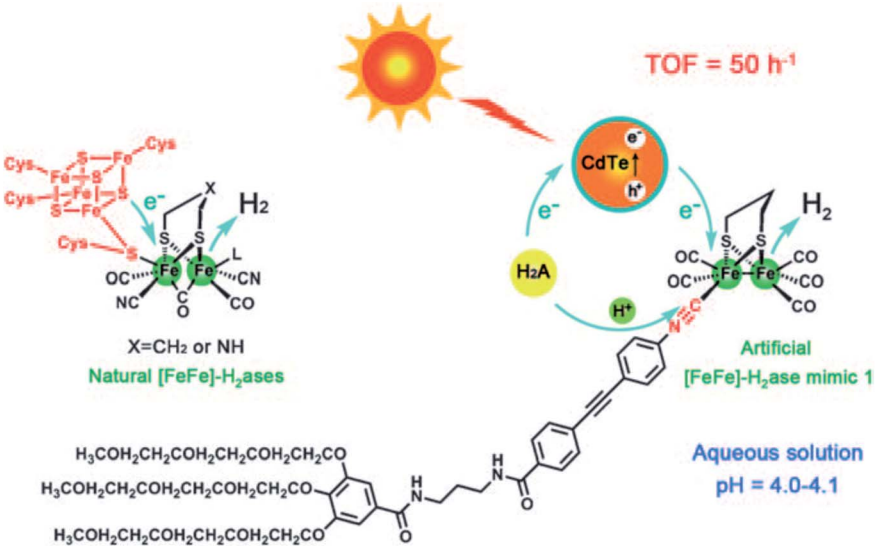

Scheme 11 Schematic diagram of the photocatalytic H_2 production system based on **MC1** and MPA-CdTe QDs. Reproduced with permission from ref. 44, Copyright 2011, Wiley-VCH.

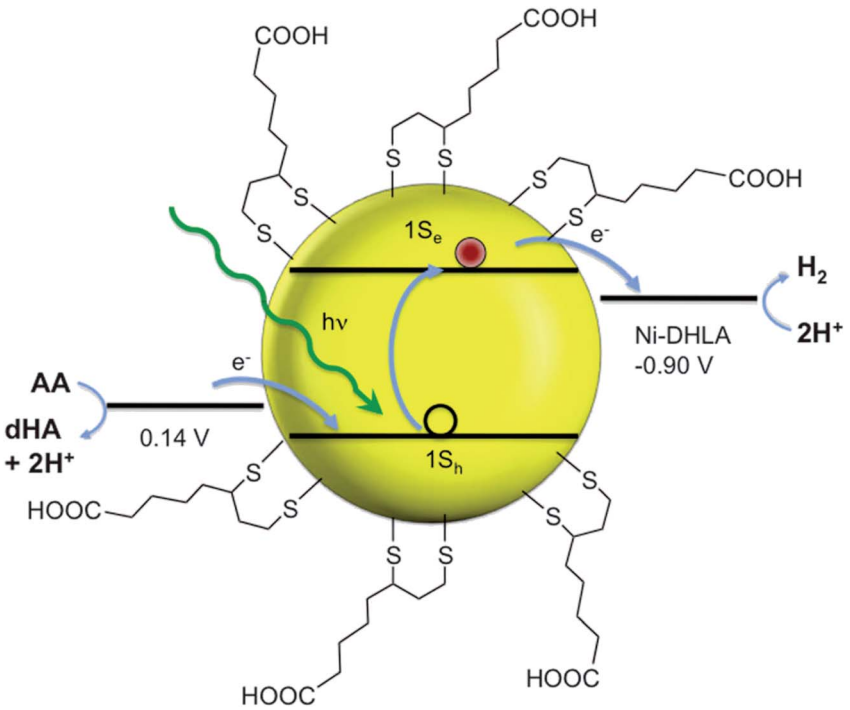

Scheme 12 Schematic diagram of the photocatalytic H_2 production by Ni^{2+}-DHLA-CdSe QDs. Reproduced with permission from ref. 80, Copyright 2012, American Association for the Advancement of Science.

semiconductors.[86–90] The efficiency of the PET from CdS to cobaloxime catalysts is controlled by the adsorption site of the catalyst at CdS, and the electrostatic interaction between them. The adsorption of cobaloxime at defects on the surface of CdS or the existence of electrostatic attraction between CdS and cobaloxime favors the PET efficiency. Wu revealed that the PET efficiency between the PS and hydrogenase mimics (**MC5** and **MC6**) could be enhanced by using CdSe QDs to replace the molecular photosensitizer $[Ru(bpy)_3]^{2+}$ in aqueous solution.[91] The system using CdSe QDs undergoes oxidative-quenching for the direct transfer of excited electrons from the conduction band of QDs to the catalyst, while the excited $[Ru(bpy)_3]^{2+}$ undergoes reductive-quenching to generate Ru^I-species and deliver electrons to the catalyst. Under the same conditions, the TONs of systems using CdSe QDs are 26 500 (for **MC5**) and 18 800 (for **MC6**), which are far higher than those of 178 (for **MC5**) and 114 (for **MC6**) by using $[Ru(bpy)_3]^{2+}$ as a PS.

In addition to the aforementioned molecular catalysts, the Co^{II}-tetraazamacrocyclic (**MC26** and **MC27**) and $[Co^{II}(bpy)_3]^{2+}$ complexes (**MC30**),[92,93] DuBois' type Ni^{II}-catalyst (**MC41**),[94] and Fe-carbonyl cluster (**MC15**)[95] were developed as molecular catalysts in combination with $CnInS_2$/ZnS, $(AgIn)_xZn_{2(1-x)}S_2$, and CdSe QDs/nano-semiconductors for photocatalytic H_2 production (Table 3). Among these systems, the combination of $CnInS_2$/ZnS QDs as a PS, **MC26** as a MC, and AA as a SED in aqueous solution at pH 5.0 shows the highest TON of 7700 under Xe lamp ($\lambda > 400$ nm) irradiation for 96 hours.

3.2 Covalent linking systems

By modification of particular anchoring groups, such as phosphonate, thiol, carboxylate, and pyridine, onto molecular catalysts, the catalysts are able to link on the surface of QDs *via* covalent bonds.[96–100] To this end, $Fe_2S_2(CO)_6$ (**MC7**),[99] phosphonate modified cobaloxime (**MC19**),[96] Co^{II}-N_2S_2 complexes (**MC33** and **MC34**),[98] and Co^{II}-tatraazabicyclo complexes (**MC28** and **MC29**) were linked to the surface of CdSe QDs,[97] CdSe/ZnS core/shell QDs, CdTe QDs, and $CuInS_2$/ZnS core/shell QDs, respectively, to form **MC@QD** type hybrid photocatalysts for photocatalytic H_2 production. The highest H_2 production TON of 14 400 was obtained by the **MC33**@CdTe system in the presence of ascorbate as a SED in water.[98] Time-resolved transient absorption spectroscopic studies revealed that a faster PET from QDs to MCs and a slower charge recombination process exist in such systems. For example, the PET from CdSe/ZnS core/shell QDs to cobaloxime (**MC19**) takes place with an average time constant of 105 ps, and the charge recombination occurs with a time constant of over 3 ns (Scheme 13).[96]

3.3 Non-covalent self-assembling systems

The formation of the **MC@QD** type system can be achieved by non-covalent interactions between MCs and QDs. Wang *et al.* reported that a sulfonate-functionalized [FeFe]-hydrogenase mimic **MC8** as a guest molecule can be included into the cavity of the β-cyclodextrin (CDSH, **L5**) host molecule modified on the surface of CdSe QDs.[101] The **MC8**@CDSH-CdSe system exhibited a faster PET and a higher H_2 production efficiency in water in comparison to the reference non-assembly systems.

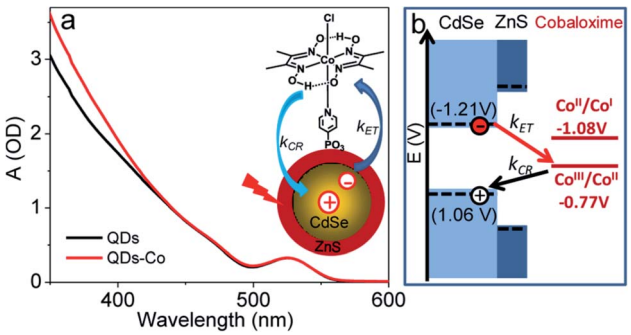

Scheme 13 (a) UV-vis absorption spectra of CdSe/ZnS core/shell QDs with (red) and without **MC19**, and the schematic structure of **MC19**@CdSe/ZnS QDs. (b) Energy diagram of CdSe/ZnS core/shell QDs and **MC19**. Reproduced with permission from ref. 96, Copyright 2012, American Chemical Society.

The TON of the assembly system is 2370, while the TON of the non-assembly system is only 358. Wu *et al.* synthesized an adamantane functionalized [FeFe]-hydrogenase mimic **MC9** and per-6-thiol-cyclodextrin (CD6SH, **L6**) modified CdSe QDs.[102] A **MC9**@CD6SH-CdSe assembly was formed driven by the strong host-guest interaction between adamantane and cyclodextrin. The H_2 production activity of the **MC9**@CD6SH-CdSe assembly in acidic aqueous solution is 122-fold higher than that of the corresponding system using QDs without the **L6** ligand. The presence of cyclodextrin can not only prevent the aggregation of the QDs under acidic conditions, but also avoid photocorrosion of the QDs by balancing the interfacial charge.

By modification of the 11-mercaptoundecanoic acid ligand (MUA, **L7**) of a long alkyl chain onto the surface of CdSe QDs, hydrophobic spaces are formed near the surface of MUA-CdSe QDs. Benefiting from this feature, a water insoluble Ni-complex (**MC43**) is able to stay in the hydrophobic spaces of MUA-CdSe QDs. A self-assembly **MC43**@MUA-CdSe system produced H_2 with a TON of 10 677 in aqueous solution.[103]

The catalytically active center in natural hydrogenase is protected by proteins. Wu *et al.* confined a [FeFe]-hydrogenase mimic **MC10** and CdTe QDs in chitosan to mimic the protein environment of the natural model (Scheme 14).[104] Chitosan was proposed to protect the QDs and the mimic in the course of photocatalysis. The H_2 production activity (TON = 52 800) and stability of the system were dramatically improved in the presence of chitosan (Table 3).

3.4 *In situ* active site formation systems

The *in situ* formation of molecular-like active sites by coordination between metal ions and QDs' surface ligand represents an alternative to construct **MC@QD** systems.[105–107] In this regard, Isimjan and Takanabe *et al.* reported that 1,2-ethanedithiol (EDT, **L8**) ligands, capped on the surface of CdS nanocrystals, are able to coordinate with Ni^{2+} ions and form $Ni(EDT)_2$ active species on the CdS surface.[105] In this system, CdS and $Ni(EDT)_2$ function as a PS and molecular-like catalyst, respectively. It produced H_2 under Xe lamp irradiation in the presence of Na_2S and Na_2SO_3 as SEDs, and a TON of 7200 based on nickel was obtained. In another study, Krauss *et al.* described that a Co^{2+}-GSH-CdSe QD (GSH = glutathione, **L9**) system, in which the active cobalt catalysts are formed through *in situ* coordination between Co^{2+} ions and surface GSH ligands, produced H_2 with a TON of 130 000 under visible light irradiation by using AA as a SED.[106]

3.5 CQD-based systems

Several hybrid AP systems for H_2 production by using CQDs as a PS were developed by Reisner's group.[108–110] The CQDs (6.8 ± 2.3 nm) with a terminal carboxylic acid were prepared by thermolysis of citric acid and were water-soluble. The photocatalytic H_2 production aqueous system composed of the CQDs as a PS, a nickel bis(diphosphine) complex (**MC41**) as a catalyst, and ethylene diamine tetraacetic acid (EDTA) as a SED, produced H_2 with a relatively short lifetime. The activity of H_2 production ceased within 4 hours, and a TON of 64 was obtained.[108] The limited stability of the system is attributed to the decomposition of the nickel catalyst caused by radicals generated by EDTA oxidation. By using a new electron donor system consisting of ascorbic acid and tris(carboxyethyl)phosphine (TCEP), the H_2 production activity of the system was improved, and a high TON of 1094 ± 61 was achieved.[109] The two-electron oxidation process of TCEP circumvents the generation of radicals in the system (Scheme 9). Recently, an analogous system composed of

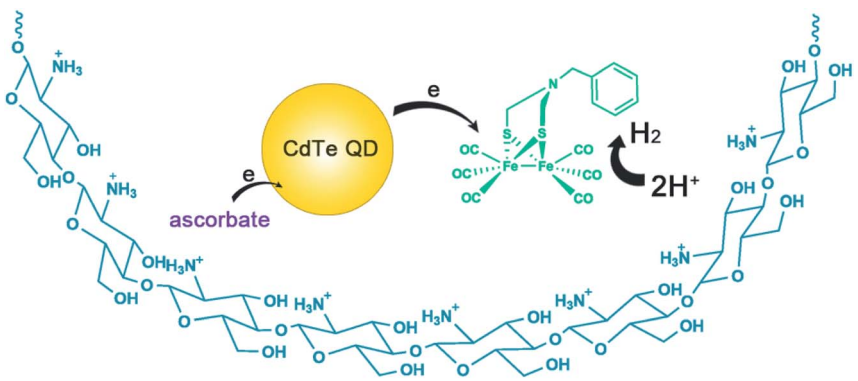

Scheme 14 Schematic diagram of the chitosan-confined H_2 photogeneration by MPA-CdTe QDs and **MC10**.

a cobalt complex (**MC26**) and CQDs in TCEP/AA aqueous system was reported. The system produced H_2 with a TON of 264 under sun irradiation for 21 days.[111]

Our group developed an artificial photosynthetic assembly (APA) of a novel hollow-rod structure by using synthetic building blocks, CQDs as a photosensitizer and PEI-Co (**MC35**) as an artificial enzyme, to mimic the structure and function of natural photosynthetic bacteria (Scheme 15).[112] The APA assemblies formed in water by the electrostatic attraction between the negatively charged CQDs and the positively charged PEI-Co (**MC35**). PEI-Co was synthesized by grafting cobalt complexes as molecular catalysts onto branched PEI. The APA features a bacteria-like shape and a hollow structure positioning light harvesting component on the surface to maximize light absorption (Scheme 16). The APA exhibits enhanced photocatalytic H_2 production within a broad pH range in aqueous solution in comparison to the corresponding non-assembly system.

3.6 Integrated ternary systems

Ternary systems are obtained by anchoring light harvesting materials and molecular catalysts onto functional materials.[113–116] We fabricated a ternary **MC21**@CdS/rGO photocatalyst (rGO referred to as reduced graphene oxide) by anchoring CdS nanocrystals and a cobaloxime catalyst **MC21** onto the surface of rGO for photocatalytic H_2 production (Scheme 17).[113] A pyrene modified cobaloxime catalyst **MC21**

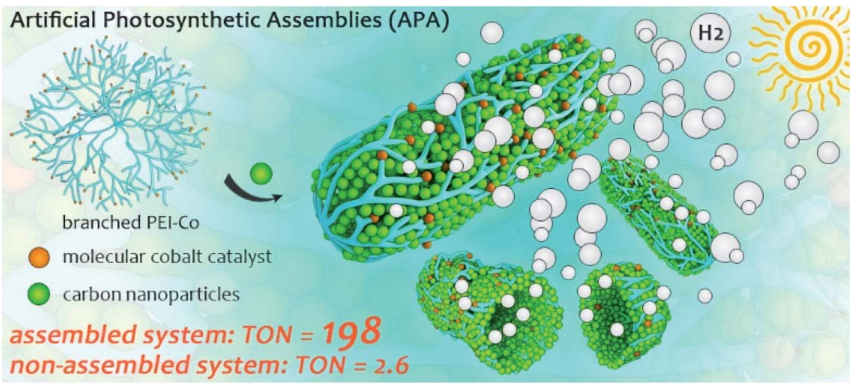

Scheme 15 Schematic diagram of photocatalytic H_2 production by the hollow-rod artificial photosynthetic assembly (APA) in water. Reproduced with permission from ref. 112, Copyright 2020, Royal Society of Chemistry.

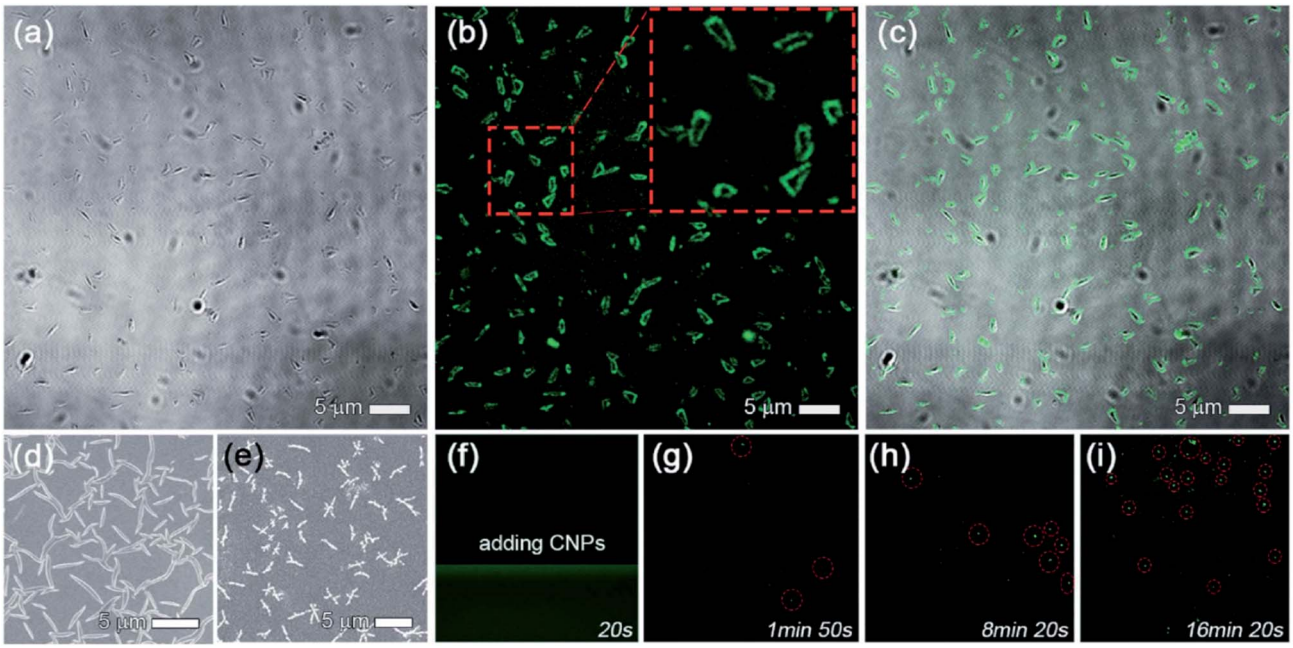

Scheme 16 (a–c) Confocal microscopy images of the APA; inset: enlarged view of the selected area (red line). The SEM images of **MC35** (d) and **MC35**@CNPs (e). (f–i) Confocal microscopy images recorded after adding CNPs into an aqueous solution of **MC35** (ref. 112). Reproduced with permission from ref. 112, Copyright 2020, Royal Society of Chemistry.

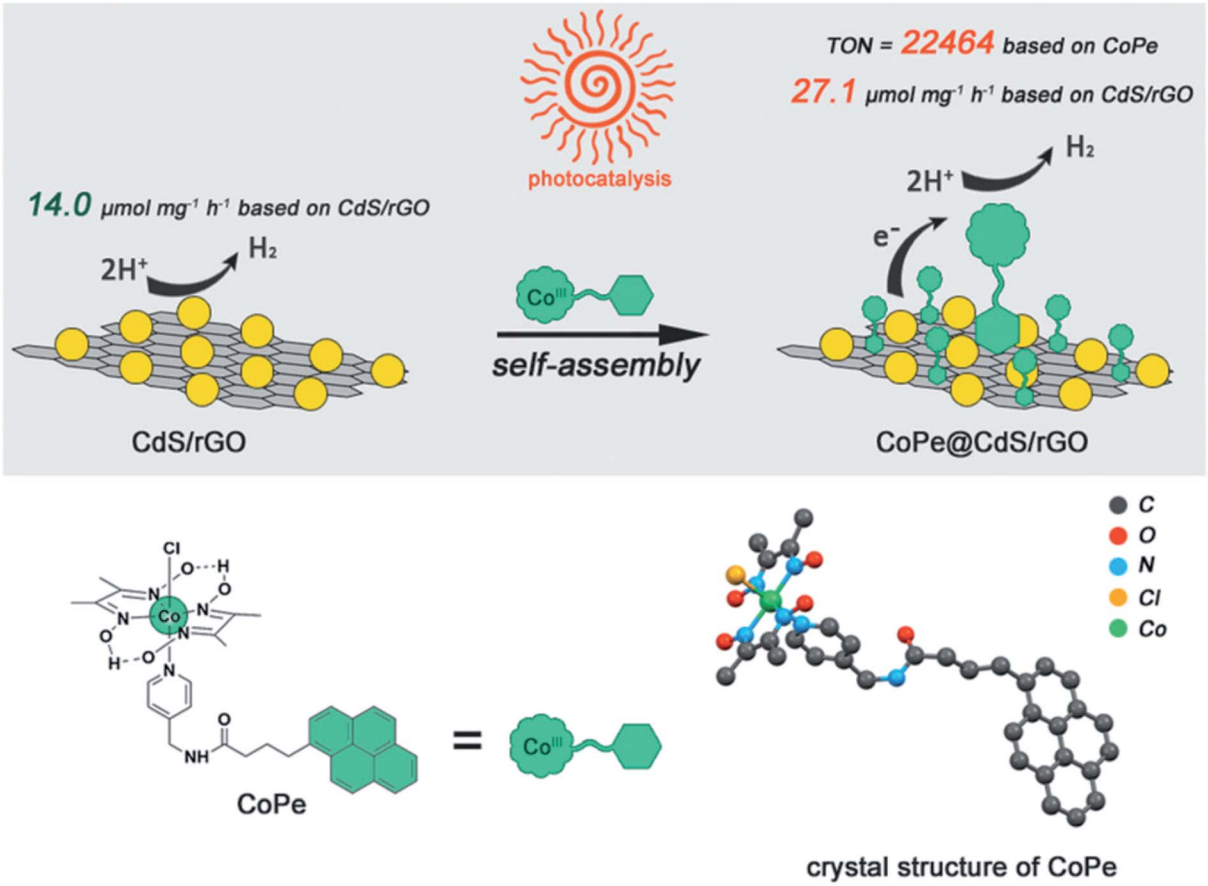

Scheme 17 Schematic diagram of the **MC21**@CdS/rGO hybrid for photocatalytic H_2 production (top). The chemical and crystal structures of **MC21** (bottom). Reproduced with permission from ref. 113, Copyright 2019, Royal Society of Chemistry.

was synthesized to facilely attach the cobalt catalyst onto the surface of rGO *via* non-covalent π–π interactions. The photocatalytic H_2 production rate of the **MC21**@CdS/rGO photocatalyst is higher than those of the non-assembled system and the pristine CdS/rGO composite under the same conditions. A TON of 22 464 was obtained by the ternary photocatalyst. Femtosecond transient absorption spectroscopic studies revealed that the PET from the excited CdS nanocrystals to cobalt catalysts occurred, and a long-lived charge-separation state formed in the ternary system.

Two CQD-based ternary systems, **MC16**/CQDs/$ZnIn_2S_4$ and **MC32**/CQDs/CN (CN = carbon nitride), were reported, in which CQDs were proposed to function as electron media to shuttle the photogenerated electrons in $ZnIn_2S_4$ or CN to the cobalt complex **MC16** or **MC32**, respectively.[114,115] The H_2 production efficiency of these two systems, **MC16**/CQDs/$ZnIn_2S_4$ and **MC32**/CQDs/CN, is 1760 μmol g^{-1} h^{-1} and 295.9 μmol g^{-1} h^{-1}, respectively. The TON based on the cobalt complex is 567 for **MC16** and 49.9 for **MC32**.

4. Hybrid AP systems for the CRR

So far, the number of reported hybrid AP systems for the CRR are less than that for the HER.[117–131] One of the main reasons, in our opinion, is that fewer molecular catalysts having activity for the CRR have been explored. Following the same strategies aforementioned, more than a dozen of hybrid AP systems for the CRR had been developed (Table 4). Molecular catalysts based on Fe^{III}, Fe^{II}, Co^{II}, Ni^{II}, Re^{I}, and Ru^{II}, and semiconductor nanocrystals, such as $CuInS_2$, CdS, CdTe, ZnSe, bimetallic sulfides, and CQDs were used in these systems. In this section, the hybrid AP systems for the CRR are divided into four subsections based on the molecular catalysts.

4.1 Fe-complexes

Weiss *et al.* constructed a hybrid system by using *meso*-tetraphenylporphyrin iron(III) chloride (**MC44**) as a catalyst, $CuInS_2$/ZnS QDs as a PS, and *N*,*N*,*N*′,*N*′-tetramethyl-*p*-phenylenediamine (TMPD) as a SED in CO_2-saturated DMSO.[117] The system produced CO with a selectivity of 84% and a TON of 58. The Fe^0 species, generated by successively accepting three electrons from the excited QDs, is assigned to the active site for CO_2 binding. Transient absorption spectroscopy revealed that the ultrafast first two electron transfer processes from the QDs to **MC44** (Fe^{III} → Fe^{II} and Fe^{II} → Fe^{I}) occur within 200 fs, and they are far more efficient than those in the corresponding systems using a molecular PS, $Ir(ppy)_3$ or 9-cyanoanthracene. Subsequently, they used a positively charged trimethylamine-functionalized

Table 4 Components, conditions, and photocatalytic efficiencies of the hybrid AP systems for the CRR

Entry	PS	MC	SED	Solvent	Light source	Irradiation time/h	Main product	TON	Selectivity/%	QY/%	Ref.
1	MPO-$CuInS_2$/ZnS	**MC44**	TMPD	DMSO	LED (λ = 450 nm)	10	CO	58*	84	N. R.	117
2	MPA-$CuInS_2$/ZnS	**MC45**	TEOA	H_2O	LED (λ = 450 nm)	30	CO	450	99	N. R.	118
3	CdS/Bi_2S_3	**MC46**	TEOA	CH_3CN/H_2O	Xe (λ > 420 nm)	4	CO	281*	24	N. R.	119
4	EF-CdS	**MC46**	TEOA	CH_3CN/H_2O	Xe (λ > 420 nm)	4	CO	4.23*	97	N. R.	120
5	$Zn_xCd_{1-x}S$	**MC46**	TEOA	CH_3CN/H_2O	Xe (λ > 420 nm)	12	CO	9.2	93	N. R.	121
6	CQDs/g-C_3N_4	**MC46**	TEOA	H_2O	Xe (λ > 420 nm)	6	CO	24.9	24.5	N. R.	122
7	MPA-CdS	**MC47**	TEOA	H_2O	Xe (λ > 420 nm)	120	CO	1380	95	N. R.	123
8	CdS	**MC48**	TEOA	CH_3CN	Xe ($\lambda \geq$ 420 nm)	10	CO	2.24	85	0.65 (420 nm)**	124
9	CdS	**MC30**	TEOA	CH_3CN	Xe (λ > 420 nm)	8	CO	4.1	87	1 (470 nm)	131
10	CdS	**MC49**	TEOA	CH_3CN/H_2O	Xe (λ > 400 nm)	N. R.	N. R.	N. R.	N. R.	N. R.	125
11	CdS	**MC50**	TEOA	CH_3CN/H_2O	Xe (λ > 400 nm)	N. R.	N. R.	N. R.	N. R.	N. R.	125
12	CdS	**MC51**	TEOA	CH_3CN/H_2O	Xe (λ > 400 nm)	N. R.	N. R.	N. R.	N. R.	N. R.	125
13	CdS	**MC52**	TEOA	CH_3CN/H_2O	Xe (λ > 400 nm)	24	CO	20	92.2	N. R.	125
14	ZnSe	**MC53**	AA	H_2O	Xe (λ > 400 nm)	20	CO	280	33	N. R.	126
15	$(CuGa)_{1-x}Zn_{2x}S$ (x = 0.7)	**MC54**	H_2O	$NaHCO_3$	Xe (λ > 390 nm)	16	CO	214	60	N. R.	127
16	MPA-$CuInS_2$	**MC55**	TEOA	DMSO	LED ($\lambda \geq$ 420 nm)	6	CO	16	N. R.	N. R.	128
17	CdS	**MC56**	TEOA	CH_3CN/H_2O	Xe (λ > 420 nm)	2	CO	0.52*	>80	1.68 (420 nm)**	130

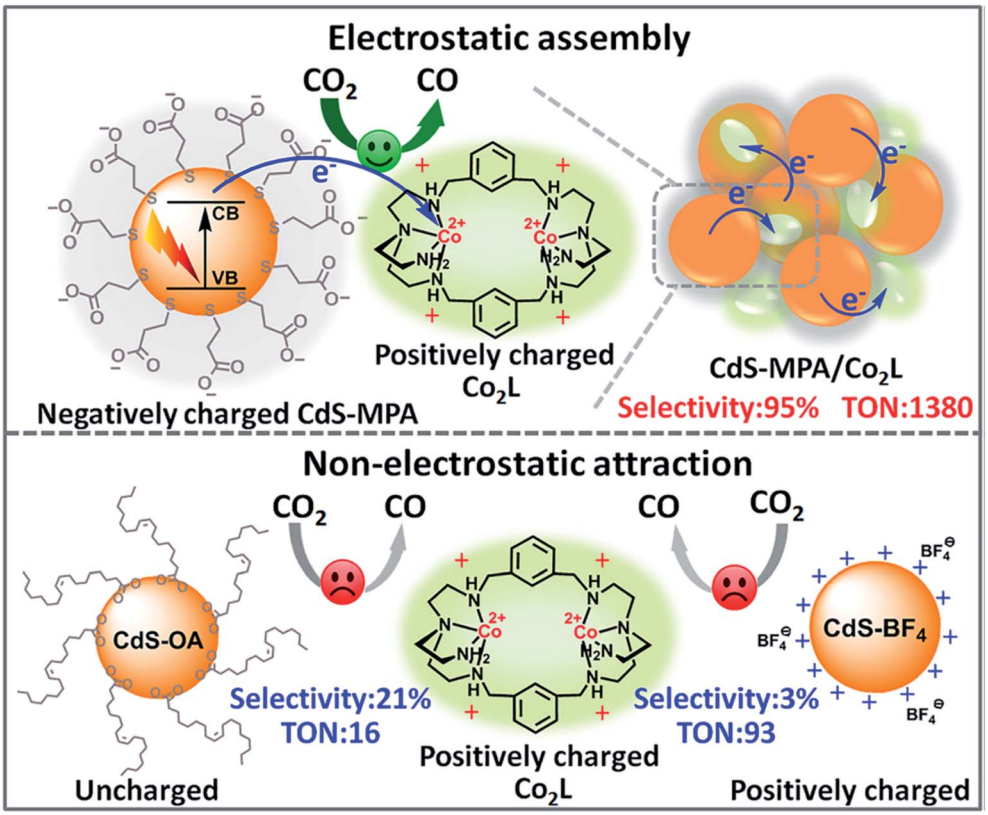

Scheme 18 Schematic diagram of CdS with different charge characteristics and the photocatalytic CO_2-to-CO conversion. Reproduced with permission from ref. 123, Copyright 2018, American Chemical Society.

tetraphenylporphyrin iron(III) chloride catalyst (**MC45**) and negatively charged $CuInS_2$/ZnS QDs to form an electrostatic self-assembly system in water.[118] The CO production TON was achieved to be 450, and the selectivity increased to 99%.

He and Chen developed a series of hybrid AP systems by using tetra(4-carboxyphenyl)porphyrin iron(III) chloride (**MC46**) as a MC.[119–122] In these systems, floccule-like EF-CdS (EF = ethylenediamine functionalization, **L10**) and Zn_xCd_{1-x} S, rod-like CdS/Bi_2S_3, and carbon dot modified g-C_3N_4 composites were used as PSs. These systems are able to convert CO_2 to CO with a selectivity varying from 24% to 97%. The highest TON of 281 (calculated based on the data given) was obtained by the

MC46/CdS/Bi_2S_3 system with a selectivity of 24%,[119] and the highest selectivity of 97% was obtained by the **MC46**/EF-CdS system with only 4 turnovers.[120]

4.2 Co-complexes

Lu *et al.* reported an electrostatic self-assembly system composed of negatively charged CdS QDs and a positively charged dinuclear cobalt complex **MC47** in water (Scheme 18).[123] The system achieved CO_2-to-CO conversion with a high selectivity of 95% and a TON of 1380, representing the highest TON so far for CO production by a hybrid system. A systematic comparison study demonstrated that the systems using uncharged or positively charged QDs are far less selective and active for CO production.

Han *et al.* developed a novel ternary system CdS/UiO-bpy/Co by the integration of CdS nanocrystals and molecular cobalt catalyst **MC48** through metal–organic framework (MOF) UiO-bpy (Scheme 19).[124] The molecular cobalt species as catalytic centers are anchored on the framework of the MOF, and the CdS nanocrystals were confined in the cavities of the MOF. The system in CH_3CN in the presence of TEOA as a SED achieved photocatalytic CO_2-to-CO conversion with a rate of 235 μmol g^{-1} h^{-1} (2 turnovers based on cobalt) and a selectivity of 85%.

4.3 Ni-complexes

A series of nickel complexes **MC49–MC52** containing different anchoring groups (R = H, COOH, PO_3H_2, and SH) were used to construct hybrid photocatalysts with CdS QDs.[125] The **MC50–MC52** are able to attach onto the surface of the QDs. The anchoring groups in these nickel complexes play a key role in controlling the selectivity of the photocatalytic CO_2-to-CO conversion in water. The system using **MC49** without an

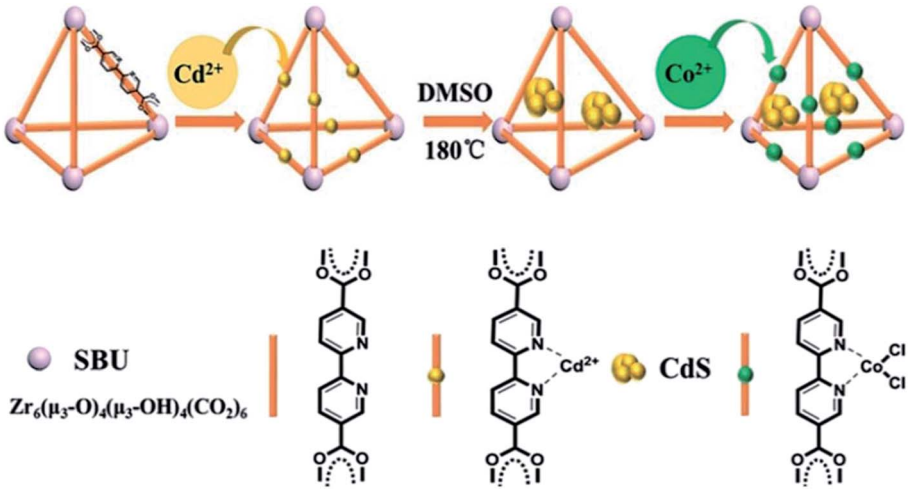

Scheme 19 Schematic diagram of the structure of the CdS/UiO-bpy/Co hybrid photocatalyst. Reproduced with permission from ref. 124, Copyright 2018, Royal Society of Chemistry.

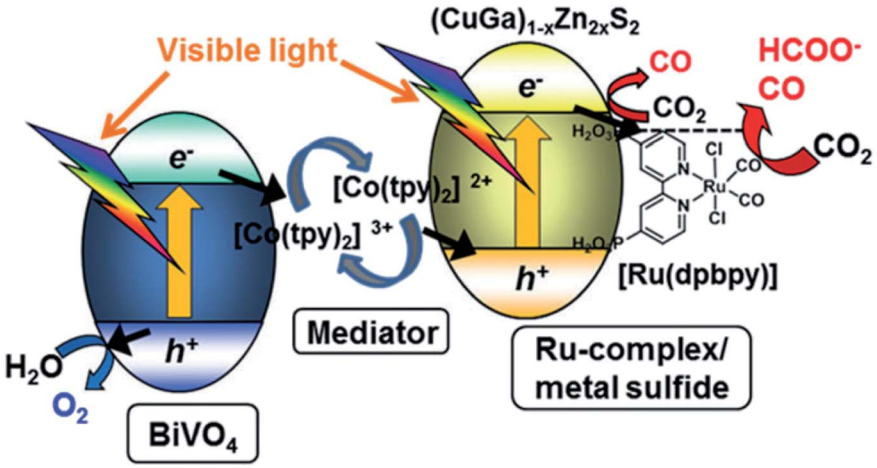

Scheme 20 Schematic diagram of the Z-schematic system for CO_2 reduction consisting of the **MC55** modified $(CuGa)_{1-x}Zn_{2x}S_2$ hybrid photocatalyst, a $BiVO_4$ photocatalyst, and a $[Co(tpy)_2]^{3+/2+}$ redox shuttle electron mediator. Reproduced with permission from ref. 127, Copyright 2018, Royal Society of Chemistry.

anchoring group produced hydrogen only. The highest CO production selectivity of over 90% and a TON of 20 were obtained by the system using thiol-functionalized complex **MC52**, which has the strongest affinity for QDs. Another hybrid self-assembly photocatalyst by anchoring a Ni-cyclam complex (**MC53**) onto the surface of ZnSe QDs was also fabricated for photocatalytic CO_2 reduction in water.[126] The TON and selectivity for CO production were achieved to be 280 and 33%, respectively. A fast PET process from the trapping state of the QDs to **MC53** occured within 186 ps.

4.4 Other metal complexes

A Z-schematic CO_2 reduction system containing Ru-complex (**MC54**) modified $(CuGa)_{1-x}Zn_{2x}S_2$ as a CO_2 reduction photocatalyst and $BiVO_4$ as a water oxidation photocatalyst was reported to realize photocatalytic CO_2 reduction by using water as an electron donor (Scheme 20).[127] The system is able to carry out CO_2 reduction and water oxidation simultaneously. The presence of the molecular Ru-catalyst improves the selectivity of CO_2 reduction. The total TON and selectivity of CO_2 reduction products (CO and $HCOO^-$) were 240 and 64%, respectively. In addition to the Ru-catalyst, a molecular rhenium complex (**MC55**) was covalently linked to $CuInS_2$ QDs for photocatalytic CO_2 reduction. A TON of 16 for CO production was reported.[128]

5. Conclusion

In conclusion, rapid and increasing research on the development of hybrid AP systems has been witnessed in the last decade. In general, an obvious improvement in photocatalytic activity and stability is observed by introducing inorganic colloidal QDs as a PS into the AP systems using molecular catalysts. The combination of colloidal QDs and MCs is one of the successful strategies for AP system construction in the past decade. In this regard, a large number of hybrid AP systems have been reported to realize the photocatalytic HER and CRR successfully. Various strategies, including physical mixing, covalent linking, non-covalent self-assembling, *in situ* active site formation, and multi-component integration, were applied to control and enhance the interaction between the QDs and the MC. On one hand, systems of higher activity, higher stability, and more complexity have been developed. On the other hand, challenges are more prominent. The efficiency and the stability of the hybrid AP systems are far less satisfactory for their applications in industry. In particular, the efficiency and selectivity of the hybrid AP systems for the CRR are low, and systems of high activity and selectivity need to be explored. The coupling of two half-reactions, protons/CO_2 reduction and water oxidation, in one system is still a big challenge. A deeper understanding of the photosynthetic mechanism, the fabrication of novel materials, and the development of a novel strategy for system construction may inspire researchers to resolve problems being faced at present.

Conflicts of interest

There are no conflicts to declare.

Acknowledgements

We are grateful for the financial support from the National Natural Science Foundation of China (21871102) and the Fundamental Research Funds for the Central Universities (2019kfyRCPY101).

References

1 J. Barber, *Chem. Soc. Rev.*, 2009, **38**, 185–196.
2 A. Stirbet, D. Lazár, Y. Guo and G. Govindjee, *Ann. Bot.*, 2020, **126**, 511–537.
3 Y. Wang, H. Yang, X. Zhang, F. Han, W. Tu and W. Yang, *Small Methods*, 2020, **4**, 1900514.
4 P. C. Hallenbeck and Y. Liu, *Int. J. Hydrogen Energy*, 2016, **41**, 4446–4454.
5 N. Armaroli and V. Balzani, *Angew. Chem., Int. Ed.*, 2007, **46**, 52–66.
6 N. S. Lewis, *Science*, 2007, **315**, 798–801.
7 Z.-J. Han and R. Eisenberg, *Acc. Chem. Res.*, 2014, **47**, 2537–2544.
8 G. Ciamician, *Science*, 1912, **36**, 385–394.
9 M. E. El-Khoulya, E. El-Mohsnawy and S. Fukuzumi, *J. Photochem. Photobiol., C*, 2017, **31**, 36–83.
10 D. R. Whang and D. H. Apaydin, *ChemPhotoChem*, 2018, **2**, 148–160.
11 S. Berardi, S. Drouet, L. Francàs, C. Gimbert-Suriñach, M. Guttentag, C. Richmond, T. Stolla and A. Llobet, *Chem. Soc. Rev.*, 2014, **43**, 7501–7519.
12 D. K. Dogutan and D. G. Nocera, *Acc. Chem. Res.*, 2019, **52**, 3143–3148.
13 Y. Tachibana, L. Vayssieres and J. R. Durrant, *Nat. Photonics*, 2012, **6**, 511–518.
14 A. Fujishima and K. Honda, *Nature*, 1972, **238**, 37–38.
15 G.-B. Chen, G. I. N. Waterhouse, R. Shi, J.-Q. Zhao, Z.-H. Li, L.-Z. Wu, C.-H. Tung and T.-R. Zhang, *Angew. Chem., Int. Ed.*, 2019, **58**, 17528–17551.
16 J. H. Montoya, L. C. Seitz, P. Chakthranont, A. Vojvodic, T. F. Jaramillo and J. K. Nørskov, *Nat. Mater.*, 2017, **16**, 70–81.
17 S. Kundu and A. Patra, *Chem. Rev.*, 2017, **117**, 712–757.
18 Y. Barak, I. Meir, A. Shapiro, Y. Jang and E. Lifshitz, *Adv. Mater.*, 2018, **30**, 1801442.
19 J. Z. Zhang and E. Reisner, *Nat. Rev. Chem.*, 2020, **4**, 6–21.
20 J.-C. Hu, M.-X. Gui, W. Xia, J. Wu, Y.-N. Zhou, N.-D. Feng, J.-W. Xiao, H.-F. Liu, L.-Z. Wu and F. Wang, *J. Mater. Chem. A*, 2019, **7**, 10475–10482.
21 Y.-Q. Wang and S.-H. Shen, *Acta Phys.-Chim. Sin.*, 2020, **36**, 1905080.
22 J. Bonin, M. Robert and M. Routier, *J. Am. Chem. Soc.*, 2014, **136**, 16768–16771.
23 X.-Q. Li, M. Wang, L. Chen, X.-N. Wang, J.-F. Dong and L.-C. Sun, *ChemSusChem*, 2012, **5**, 913–919.
24 T. Lazarides, T. McCormick, P.-W. Du, G.-G. Luo, B. Lindley and R. Eisenberg, *J. Am. Chem. Soc.*, 2009, **131**, 9192–9194.
25 H. Rao, L. C. Schmidt, J. Bonin and M. Robert, *Nature*, 2017, **548**, 74–77.

26 C.-Y. Zhu, Y.-Q. Zhang, R.-Z. Liao, W. Xia, J.-C. Hu, J. Wu, H.-F. Liu and F. Wang, *Dalton Trans.*, 2018, **47**, 13142–13150.
27 F. Wang, B. Cao, W.-P. To, C.-W. Tse, K. Li, X.-Y. Chang, C. Zang, S. L. Chan and C.-M. Che, *Catal. Sci. Technol.*, 2016, **6**, 7408–7420.
28 Y.-J. Yuan, Z.-T. Yu, D.-Q. Chen and Z.-G. Zou, *Chem. Soc. Rev.*, 2017, **46**, 603–631.
29 V. Artero, M. Chavrot-Kerlidou and M. Fontecave, *Angew. Chem., Int. Ed.*, 2011, **50**, 2–31.
30 W.-J. Sun, J.-Q. Lin, X.-M. Liang, J.-Y. Yang, B.-C. Ma and Y. Ding, *Acta Phys.-Chim. Sin.*, 2020, **36**, 1905025.
31 J. Bonin, A. Maurin and M. Robert, *Coord. Chem. Rev.*, 2017, **334**, 184–198.
32 W. Xia, Ji. Wu, J.-C. Hu, S.-S. Sun, M.-D. Li, H.-F. Liu, M.-H. Lan and F. Wang, *ChemSusChem*, 2019, **12**, 4617–4622.
33 J. L. White, M. F. Baruch, J. E. Pander, Y. Hu, I. C. Fortmeyer, J. E. Park, T. Zhang, K. Liao, Ji. Gu, Y. Yan, T. W. Shaw, E. Abelev and A. B. Bocarsly, *Chem. Rev.*, 2015, **115**, 12888–12935.
34 K. Li, B. Peng and T.-Y. Peng, *ACS Catal.*, 2016, **6**, 7485–7527.
35 S. Cao, C.-J. Wang, W.-F. Fu and Y. Chen, *ChemSusChem*, 2017, **10**, 4306–4323.
36 W. T. Eckenhoff and R. Eisenberg, *Dalton Trans.*, 2012, **41**, 13004–13021.
37 S. Fukuzumi, Y. Yamada, T. Suenobu, K. Ohkuboa and H. Kotan, *Energy Environ. Sci.*, 2011, **4**, 2754–2766.
38 T. R. Simmons, G. Berggrena, M. Bacchi and M. Fontecavea, *Coord. Chem. Rev.*, 2014, **270**, 127–150.
39 K. E. Dalle, J. Warnan, J. J. Leung, B. Reuillard, I. S. Karmel and E. Reisner, *Chem. Rev.*, 2019, **119**, 2752–2875.
40 A. Hasani, M. Tekalgne, Q. V. Le, H. W. Jang and S. Y. Kim, *J. Mater. Chem. A*, 2019, **7**, 430–454.
41 X.-B. Li, C.-H. Tung and L.-Z. Wu, *Nat. Rev. Chem.*, 2018, **2**, 160–173.
42 R. Burke, K. L. Bren and T. D. Krauss, *J. Chem. Phys.*, 2021, **154**, 030901.
43 Z. Wang, C. Li and K. Domen, *Chem. Soc. Rev.*, 2019, **48**, 2109–2125.
44 F. Wang, W.-G. Wang, X.-J. Wang, H.-Y. Wang, C.-H. Tung and L.-Z. Wu, *Angew. Chem., Int. Ed.*, 2011, **50**, 3193–3197.
45 F. E. Osterloh, *ACS Energy Lett.*, 2017, **2**, 445–453.
46 A. J. Nozik, *Appl. Phys. Lett.*, 1977, **30**, 567–569.
47 A. J. Bard, *J. Photochem.*, 1979, **10**, 59–75.
48 F. Wang, W.-G. Wang, H.-Y. Wang, G. Si, C.-H. Tung and L.-Z. Wu, *ACS Catal.*, 2012, **2**, 407–416.
49 S. H. Lee, D. S. Choi, S. K. Kuk and C. B. Park, *Angew. Chem., Int. Ed.*, 2018, **57**, 7958–7985.
50 S. Fukuzumi, K. Ohkubo and T. Suenobu, *Acc. Chem. Res.*, 2014, **47**, 1455–1464.
51 Y.-Q. Hou, X. Zhang, K.-P. Chen, D.-Y. Liu, Z.-J. Wang, Q.-Y. Liu, J.-Z. Zhao and A. Barbon, *J. Mater. Chem. C*, 2019, **7**, 12048–12074.
52 L. E. Brus, *J. Chem. Phys.*, 1984, **80**, 4403–4409.
53 C. Burda, X.-B. Chen, R. Narayanan and M. A. El-Sayed, *Chem. Rev.*, 2005, **105**, 1025–1102.
54 P. Wu and X.-P. Yan, *Chem. Soc. Rev.*, 2013, **42**, 5489–5521.
55 S. Y. Lim, W. Shen and Z. Gao, *Chem. Soc. Rev.*, 2015, **44**, 362–381.
56 C. Hu, M. Li, J. Qiu and Y.-P. Sun, *Chem. Soc. Rev.*, 2019, **48**, 2315–2337.
57 M. Lan, S. Zhao, S. Wu, X. Wei, Y. Fu, J. Wu, P. Wang and W. Zhang, *Nano Res.*, 2019, **12**, 2576–2583.
58 C. Hu, M.-Y. Li, J.-S. Qiu and Y.-P. Sun, *Chem. Soc. Rev.*, 2019, **48**, 2315–2337.
59 L.-J. Chen, G. Chen, C.-F. Leung, S.-M. Yiu, C.-C. Ko, E. Anxolabéhère-Mallart, M. Robert and T.-C. Lau, *ACS Catal.*, 2015, **5**, 356–364.
60 Y.-L. Li and T. B. Rauchfuss, *Chem. Rev.*, 2016, **12**, 7043–7077.
61 V. Artero, M. Chavarot-Kerlidou and M. Fontecave, *Angew. Chem., Int. Ed.*, 2011, **50**, 2–31.
62 A. Fihri, V. Artero, M. Razavet, C. Baffert, W. Leibl and M. Fontecave, *Angew. Chem., Int. Ed.*, 2008, **47**, 564–567.
63 C. Tard and C. J. Pickett, *Chem. Rev.*, 2009, **109**, 2245–2274.
64 N. Kaeffer, M. Chavarot-Kerlidou and V. Artero, *Acc. Chem. Res.*, 2015, **48**, 1286–1295.
65 J. L. Dempsey, B. S. Brunschwig, J. R. Winkler and H. B. Gray, *Acc. Chem. Res.*, 2009, **42**, 1995–2004.
66 T. M. McCormick, Z.-J. Han, D. J. Weinberg, W. W. Brennessel, P. L. Holland and R. Eisenberg, *Inorg. Chem.*, 2011, **50**, 10660–10666.
67 P.-W. Du, K. Knowles and R. Eisenberg, *J. Am. Chem. Soc.*, 2008, **130**, 12576–12577.
68 P.-W. Du, J. Schneider, G.-G. Luo, W. W. Brennessel and R. Eisenberg, *Inorg. Chem.*, 2009, **48**, 4952–4962.
69 T. Lazarides, T. McCormick, P.-W. Du, G.-G. Luo, B. Lindley and R. Eisenberg, *J. Am. Chem. Soc.*, 2009, **131**, 9192–9194.
70 M. L. Helm, M. P. Stewart, R. M. Bullock, M. R. DuBois and D. L. DuBois, *Science*, 2011, **333**, 863–866.
71 M. P. McLaughlin, T. M. McCormick, R. Eisenberg and P. L. Holland, *Chem. Commun.*, 2011, **47**, 7989–7991.
72 F. Wang, *ChemSusChem*, 2017, **10**, 4393–4402.
73 H. Rao, C.-H. Lim, J. Bonin, G. M. Miyake and M. Robert, *J. Am. Chem. Soc.*, 2018, **140**, 17830–17834.
74 J. Bonin, A. Maurin and M. Robert, *Coord. Chem. Rev.*, 2017, **334**, 184–198.
75 Y.-N. Wang, K.-C. Lau, W. W. Y. Lam, W.-L. Man, C.-F. Leung and T.-C. Lau, *Inorg. Chem.*, 2009, **48**, 400–406.
76 E. D. Cline, S. E. Adamson and S. Bernhard, *Inorg. Chem.*, 2008, **47**, 10378–10388.
77 F. Wang, W.-J. Liang, J.-X. Jian, C.-B. Li, B. Chen, C.-H. Tung and L.-Z. Wu, *Angew. Chem., Int. Ed.*, 2013, **52**, 8134–8138.
78 W.-J. Liang, F. Wang, M. Wen, J.-X. Jian, X.-Z. Wang, B. Chen, C.-H. Tung and L.-Z. Wu, *Chem.–Eur. J.*, 2015, **21**, 3187–3192.
79 M. Wen, X.-B. Li, J.-X. Jian, X.-Z. Wang, H.-L. Wu, B. Chen, C.-H. Tung and L.-Z. Wu, *Sci. Rep.*, 2016, **6**, 29851–29858.
80 Z.-J. Han, F. Qiu, R. Eisenberg, P. L. Holland and T. D. Krauss, *Science*, 2012, **338**, 1321–1324.

81 A. Das, Z.-J. Han, M. G. Haghighi and R. Eisenberg, *Proc. Natl. Acad. Sci. U. S. A.*, 2013, **110**, 16716–16723.
82 A. Das, Z.-J. Han, W. W. Brennessel, P. L. Holland and R. Eisenberg, *ACS Catal.*, 2015, **5**, 1397–1406.
83 H.-J. Lv, T. P. A. Ruberu, V. E. Fleischauer, W. W. Brennessel, M. L. Neidig and R. Eisenberg, *J. Am. Chem. Soc.*, 2016, **138**, 11654–11663.
84 W. R. McNamara, Z.-J. Han, C.-J. Yin, W. W. Brennessel, P. L. Holland and R. Eisenberg, *Proc. Natl. Acad. Sci. U. S. A.*, 2012, **109**, 15594–15599.
85 W. R. McNamara, Z.-J. Han, P. J. Alperin, W. W. Brennessel, P. L. Holland and R. Eisenberg, *J. Am. Chem. Soc.*, 2011, **133**, 15368–15371.
86 F.-Y. Wen, J.-H. Yang, X. Zong, B.-J. Ma, D.-G. Wang and C. Li, *J. Catal.*, 2011, **281**, 318–324.
87 F.-Y. Wen, X.-L. Wang, L. Huang, G.-J. Ma, J.-H. Yang and C. Li, *ChemSusChem*, 2012, **5**, 849–853.
88 Y. Ye, Y.-X. Xu, L. Huang, D.-Y. Fan, Z.-C. Feng, X.-L. Wang and C. Li, *Phys. Chem. Chem. Phys.*, 2016, **18**, 17389–17397.
89 Y.-X. Xu, Y. Ye, T.-F. Liu, X.-L. Wang, B.-Q. Zhang, M. Wang, H.-X. Han and C. Li, *J. Am. Chem. Soc.*, 2016, **138**, 10726–10729.
90 Y.-X. Xu, R.-T. Chen, Z. Li, A.-L. Li, H.-X. Han and C. Li, *ACS Appl. Mater. Interfaces*, 2017, **9**, 23230–23237.
91 J.-X. Jian, C. Ye, X.-Z. Wang, M. Wen, Z.-J. Li, X.-B. Li, B. Chen, C.-H. Tung and L.-Z. Wu, *Energy Environ. Sci.*, 2016, **9**, 2083–2089.
92 M. Sandroni, R. Gueret, K. D. Wegner, P. Reiss, J. Fortage, D. Aldakov and M.-N. Collomb, *Energy Environ. Sci.*, 2018, **11**, 1752–1761.
93 Y.-J. Yuan, D.-Q. Chen, M. Xiong, J.-S. Zhong, Z.-Y. Wan, Y. Zhou, S. Liu, Z.-T. Yub, L.-X. Yang and Z.-G. Zou, *Appl. Catal., B*, 2017, **204**, 58–66.
94 Y. Zhou, S. Yang and J. Huang, *Phys. Chem. Chem. Phys.*, 2017, **19**, 7471–7475.
95 C.-S. Li, A. Rahaman, W.-H. Lin, H. Mourad, J. Meng, A. Honarfar, M. Abdellah, M.-Y. Guo, M. G. Richmond, K.-B. Zheng and E. Nordlander, *ChemSusChem*, 2020, **13**, 3252–3260.
96 J.-E. Huang, K. L. Mulfort, P.-W. Du and L.-X. Chen, *J. Am. Chem. Soc.*, 2012, **134**, 16472–16475.
97 C.-M. Nie, W.-J. Ni, L.-L. Gong, J. Jiang, J.-H. Wang and M. Wang, *J. Mater. Chem. A*, 2019, **7**, 27432–27440.
98 K. Han, M. Wang, S. Zhang, S.-L. Wu, Y. Yang and L.-C. Sun, *Chem. Commun.*, 2015, **51**, 7008–7011.
99 C.-B. Li, Z.-J. Li, S. Yu, G.-X. Wang, F. Wang, Q.-Y. Meng, B. Chen, K. Feng, C.-H. Tung and L.-Z. Wu, *Energy Environ. Sci.*, 2013, **6**, 2597–2602.
100 W.-W. Zhao, Y. Huang, Y. Liu, L.-M. Cao, F. Zhang, Y.-M. Guo and B. Zhang, *Chem.–Eur. J.*, 2016, **22**, 15049–15057.
101 M.-L. Cheng, M. Wang, S. Zhang, F.-Y. Liu, Y. Yang, B.-S. Wan and L.-C. Sun, *Faraday Discuss.*, 2017, **198**, 197–209.
102 X.-B. Li, J.-X. Jian, X.-Z. Wang, Y. Wang, S.-G. Xia, C.-H. Tung and L.-Z. Wu, *Sol. RRL*, 2021, **5**, 2000474.
103 Y.-J. Le, S. Liu, G.-L. Hu, R. Hu, R.-T. Yan, Y.-B. Lu and H.-Y. Wang, *Int. J. Hydrogen Energy*, 2019, **44**, 20079–20084.
104 J.-X. Jian, Q. Liu, Z.-J. Li, F. Wang, X.-B. Li, C.-B. Li, B. Liu, Q.-Y. Meng, B. Chen, K. Feng, C.-H. Tung and L.-Z. Wu, *Nat. Commun.*, 2013, **4**, 2695.
105 W.-L. Yu, T. Isimjan, S. D. Gobbo, D. H. Anjum, S. Abdel-Azeim, L. Cavallo, A. T. Garcia-Esparza, K. Domen, W. Xu and K. Takanabe, *ChemSusChem*, 2014, **7**, 2575–2583.
106 R. Burke, S. Chakraborty, K. P. McClelland, J. Jelusic, E. M. Matson, K. L. Bren and T. D. Krauss, *Chem. Commun.*, 2021, **57**, 2053–2056.
107 F. Qiu, Z.-j. Han, J. J. Peterson, M. Y. Odoi, K. L. Sowers and T. D. Krauss, *Nano Lett.*, 2016, **16**, 5347–5352.
108 B. C. M. Martindale, G. A. M. Hutton, C. A. Caputo and E. Reisner, *J. Am. Chem. Soc.*, 2015, **137**, 6018–6025.
109 B. C. M. Martindale, E. Joliat, C. Bachmann, R. Alberto and E. Reisner, *Angew. Chem., Int. Ed.*, 2016, **55**, 9402–9406.
110 B. C. M. Martindale, G. A. M. Hutton, C. A. Caputo, S. Prantl, R. Godin, J. R. Durrant and E. Reisner, *Angew. Chem., Int. Ed.*, 2017, **56**, 6459–6463.
111 K. Ladomenou, G. Landrou, G. Charalambidis, E. Nikoloudakis and A. G. Coutsolelos, *Sustainable Energy Fuels*, 2021, **5**, 449–458.
112 J. Wu, W. Xia, M.-H. Lan, X.-J. Xing, J.-C. Hu, L. Huang, J. Liu, Y.-Y. Ren, H.-F. Liu and F. Wang, *J. Mater. Chem. A*, 2020, **8**, 21690–21699.
113 J.-C. Hu, S. Sun, M.-D. Li, W. Xia, J. Wu, H. Liu and F. Wang, *Chem. Commun.*, 2019, **55**, 14490–14493.
114 Y. Ding, Y.-H. Gao and Z.-H. Li, *Appl. Surf. Sci.*, 2018, **462**, 255–262.
115 Y.-X. Zhang and W.-D. Zhang, *Carbon*, 2019, **145**, 488–500.
116 H.-K. Zhao, X.-X. Li, M.-Y. Zheng, X. Zhao, Q. Zhang, Y. Luo and W.-L. Fan, *Nanoscale*, 2020, **12**, 11267–11279.
117 S.-C. Lian, M. S. Kodaimati, D. S. Dolzhnikov, R. Calzada and E. A. Weiss, *J. Am. Chem. Soc.*, 2017, **139**, 8931–8938.
118 S.-C. Lian, M. S. Kodaimati and E. A. Weiss, *ACS Nano*, 2018, **12**, 568–575.
119 P. Lia, X.-H. Zhang, C.-C. Hou, Y. Chen and T. He, *Appl. Catal., B*, 2018, **238**, 656–663.
120 P. Lia, C.-C. Hou, X.-H. Zhang, Y. Chen and T. He, *Appl. Surf. Sci.*, 2018, **459**, 292–299.
121 P. Li, X.-H. Zhang, C.-C. Hou, L. Lin, Y. Chen and T. He, *Phys. Chem. Chem. Phys.*, 2018, **20**, 16985–16991.
122 X.-H. Zhang, L. Lin, D. Qu, J.-G. Yang, Y.-X. Weng, Z. Wang, Z.-C. Sun, Y. Chen and T. He, *Appl. Catal., B*, 2020, **265**, 118595.
123 Q.-Q. Bi, J.-W. Wang, J.-X. Lv, J. Wang, W. Zhang and T.-B. Lu, *ACS Catal.*, 2018, **8**, 11815–11821.
124 C.-J. Chen, T.-B. Wu, H.-H. Wu, H.-Z. Liu, Q.-L. Qian, Z.-M. Liu, G.-Y. Yang and B.-X. Han, *Chem. Sci.*, 2018, **9**, 8890–8894.
125 M. F. Kuehnel, K. L. Orchard, K. E. Dalle and E. Reisner, *J. Am. Chem. Soc.*, 2017, **139**, 7217–7223.
126 M. F. Kuehnel, C. D. Sahm, G. Neri, J. R. Lee, K. L. Orchard, A. J. Cowan and E. Reisner, *Chem. Sci.*, 2018, **9**, 2501–2509.
127 T. M. Suzuki, S. Yoshino, T. Takayama, A. Iwase, A. Kudo and T. Morikawa, *Chem. Commun.*, 2018, **54**, 10199–10202.

128 J. Huang, M. G. Gatty, B. Xu, P. B. Pati, A. S. Etman, L. Tian, J.-L. Sun, L. Hammarström and H.-N. Tian, *Dalton Trans.*, 2018, **47**, 10775–10783.
129 Y.-P. Bao, J. Wang, Q. Wang, X.-F. Cui, R. Long and Z.-Q. Li, *Nanoscale*, 2020, **12**, 2507–2514.
130 J.-L. Lin, B. Qin and Z.-X. Fang, *Catal. Lett.*, 2019, **149**, 25–33.
131 Z.-G. Chai, Q. Li and D.-S. Xu, *RSC Adv.*, 2014, **4**, 44991–44995.